Research Square

Preprints are preliminary reports that have not undergone peer review.
They should not be considered conclusive, used to inform clinical practice,
or referenced by the media as validated information.

Gut-derived circulating bacterial vesicles reduce systemic carbapenem exposure and sustain extraintestinal infections

Zhen Shen

zhenshen@shsmu.edu.cn

Renji Hospital, School of Medicine, Shanghai Jiao Tong University

Guoxiu Xiang

Ren Ji Hospital

Jialin Huang

Department of Neurosurgery, Renji Hospital, Shanghai Jiao Tong University School of Medicine

Junying Zhu

Department of Laboratory Medicine, Renji Hospital, School of Medicine, Shanghai Jiao Tong University

Ziyu Yang

Ren Ji Hospital

Qianqian Gao

Department of Laboratory Medicine, Renji Hospital, School of Medicine, Shanghai Jiao Tong University

Tianchi Chen

Ren Ji Hospital

Yan Song

Renji Hospital

Xilong Zhang

Ren Ji Hospital, Shanghai Jiao Tong University School of Medicine

Yiwei Zhu

Department of Critical Care Medicine, Renji Hospital, School of Medicine, Shanghai Jiao Tong University

Chen Wang

Department of Laboratory Medicine, Renji Hospital, School of Medicine, Shanghai Jiao Tong University

Juanxiu Qin

Renji Hospital, School of Medicine , Shanghai Jiaotong University

Haomin Zhang

Department of Laboratory Medicine, Renji Hospital, School of Medicine, Shanghai Jiao Tong University

Hua Wang

Department of Laboratory Medicine, Renji Hospital, School of Medicine, Shanghai Jiao Tong University

Min Li
Ren Ji Hospital, School of Medicine, Shanghai Jiao Tong University, Shanghai, China
https://orcid.org/0000-0002-8571-2909

Article

Keywords:

Posted Date: November 11th, 2026

DOI: https://doi.org/10.21203/rs.3.rs-11583209/v1

License: This work is licensed under a Creative Commons Attribution 4.0 International License.
Read Full License

Additional Declarations: There is **NO** Competing Interest.

Gut-derived circulating bacterial vesicles reduce systemic carbapenem exposure and sustain extraintestinal infections

Guoxiu Xiang[1,6], Jialin Huang[2,3,6], Junying Zhu[1,6], Ziyu Yang[1], Qianqian Gao[1], Tianchi Chen[1], Yan Song[1], Xilong Zhang[1], Yiwei Zhu[4], Chen Wang[1], Juanxiu Qin[1], Haomin Zhang[1], Hua Wang[1]✉, Min Li[1,5]✉, Zhen Shen[1]✉

[1]Department of Laboratory Medicine, Renji Hospital, School of Medicine, Shanghai Jiao Tong University, Shanghai, China

[2]Department of Neurosurgery, Renji Hospital, Shanghai Jiao Tong University School of Medicine, Shanghai, China

[3]Shanghai Institute of Head Trauma, Shanghai, China

[4]Department of Critical Care Medicine, Renji Hospital, School of Medicine, Shanghai Jiao Tong University, Shanghai, China

[5]School of Nursing, Shanghai Jiao Tong University, Shanghai, China

[6]These authors contributed equally: Guoxiu Xiang, Junying Zhu, Ziyu Yang.

✉Corresponding authors:

zhenshen@shsmu.edu.cn (Zhen Shen)

rjlimin@shsmu.edu.cn (Min Li)

renjijywh@shsmu.edu.cn (Hua Wang)

Abstract

Infections frequently persist despite appropriate antibiotic therapy against susceptible pathogens. While unexplained treatment failure is typically linked to the pathogen itself or the local infection environment, we show that spatially distinct colonized resistant populations can undermine systemic therapy. In a 1,028-patient cohort, fecal colonization with carbapenem-resistant *Escherichia coli* (CREC) independently compromised carbapenem efficacy against susceptible extraintestinal *Enterobacterales*. Mechanistically, CREC secretes the carbapenemase NDM exclusively via outer membrane vesicles (OMVs). Following intestinal barrier injury, NDM-loaded OMVs translocate into the circulation. These circulating vesicles resist plasma inactivation and accelerate systemic carbapenem clearance, dropping effective drug exposure below therapeutic thresholds to rescue distant susceptible pathogens without genetic transfer. This protection requires porin-mediated antibiotic entry into OMVs and is amplified by carbapenem exposure, which increases vesicle release and enriches NDM cargo. NDM-stable aztreonam-avibactam and non-β-lactam amikacin bypass this vesicle sink and retain *in vivo* efficacy. Thus, gut microbiota resistance acts as a remote pharmacological sink via circulating bacterial vesicles, compromising antibiotic therapy against distant susceptible pathogens.

Enterobacterales, particularly *Escherichia coli and Klebsiella pneumoniae*, are among the leading causes of healthcare-associated infections[1,2]. While antimicrobial susceptibility testing routinely guides therapy, infections can persist despite *in vitro* susceptibility and appropriate antibiotic treatment. Such clinical failure is typically attributed to antibiotic persistence[3], biofilm formation[4], or poor drug penetration at the site of infection[5]. However, these mechanisms rely entirely on the infecting bacterial population or the local infection environment. Whether colonizing resistant populations outside the infection site can alter systemic antibiotic exposure to compromise the treatment of a distant, susceptible pathogen remains poorly understood.

The human gut is a major reservoir of antimicrobial resistance, particularly in hospitalized patients[6]. Resistant *Enterobacterales* can persist in the intestine for months[7], and the clinical importance of intestinal carriage has mainly been studied in relation to transmission and subsequent infection by the colonizing bacteria[8,9]. It remains unclear whether a resistant gut population can alter systemic antibiotic activity and compromise treatment of a distant susceptible pathogen, without directly causing infection or transferring resistance genes.

One potential bridge between the gut and systemic compartments is the release of bacterial outer membrane vesicles (OMVs) by Gram-negative bacteria. These membrane-bound particles deliver bacterial proteins, including antibiotic-degrading enzymes, into the extracellular environment[10,11]. β-lactamases packaged into OMVs retain their catalytic activity and can protect neighboring susceptible bacteria through

extracellular drug hydrolysis[12,13,14]. New Delhi metallo-β-lactamase (NDM) is highly prone to this packaging because it is a lipidated, membrane-anchored carbapenemase[12]. Previous work has shown that NDM-containing OMVs can hydrolyze β-lactams and protect susceptible bacteria *in vitro* and in an invertebrate infection model[13,14]. Bacterial vesicles of gut origin have also been detected in human blood[15,16]. However, whether carbapenemase-loaded OMVs released from gut-colonizing bacteria can reach the circulation and alter systemic antibiotic exposure, remains unknown.

Here, we show that intestinal colonization with carbapenem-resistant *Escherichia coli* (CREC) is independently associated with the clinical failure of carbapenem therapy against susceptible extraintestinal *Enterobacterales*, based on a retrospective cohort of 1,028 patients. We found that fecal CREC uniformly carried the bla_{NDM} gene and secretes NDM exclusively via OMVs. Following intestinal barrier injury, NDM-loaded OMVs could enter the circulation, accelerate systemic carbapenem degradation, and reduce effective drug exposure below therapeutic thresholds. These results define a vesicle-mediated mechanism where antimicrobial resistance in the gut microbiota acts as a remote pharmacological sink, compromising systemic antibiotic therapy against fully susceptible pathogens.

Fecal CREC colonization drives persistent extraintestinal infection and confers OMV-mediated carbapenem protection

To understand why seemingly appropriate antibiotic therapy fails in some patients, we analyzed a cohort of 1,028 hospitalized individuals with carbapenem-susceptible

Enterobacterales infections, comprising 262 persistent and 766 non-persistent cases (**Fig. 1a**). We first asked if intrinsic pathogen properties could explain this persistence. Phylogenetic analysis of the infecting *Klebsiella pneumoniae* and *Escherichia coli* strains showed either clonal replacement or minimal single-nucleotide polymorphism (SNP) accumulation within a single clone, indicating that pathogen microevolution does not drive clinical persistence (**Extended data Fig. 1 and Fig. 2**). Furthermore, isolates from both clinical groups exhibited similar minimum inhibitory concentration (MIC) distributions for standard antibiotics and comparable meropenem-mediated killing *in vitro* (**Extended data Fig. 3**). These findings rule out reduced pathogen susceptibility as the primary cause of treatment failure.

Multivariate analysis of host and infection variables identified fecal colonization with carbapenem-resistant *E. coli* (CREC) as the strongest independent risk factor for persistent infection (**Fig. 1b**, **Extended data Fig. 4a**, **b**, and **Table 1** and **2**). Genomic analysis of fecal CREC isolates from this cohort revealed a polyclonal population structure where all isolates harbored the carbapenemase gene bla_{NDM}, predominantly $bla_{\text{NDM-5}}$ (92.9%) (**Fig. 1c**). Because NDM can hydrolyze nearly all β-lactam antibiotics[17], we hypothesized that gut-colonizing CREC might release NDM to protect susceptible pathogens.

Unlike soluble periplasmic β-lactamases, NDM is a lipidated lipoprotein anchored to the outer membrane[12]. Subcellular fractionation of CREC cultures confirmed that NDM is released into the extracellular environment exclusively via outer membrane vesicles (OMVs) (**Fig. 1d-h**). Both NDM protein and

carbapenem-hydrolyzing activity partitioned strictly with the >100 kDa vesicle pellet and density-gradient-purified OMVs, and were undetectable in vesicle-depleted soluble fractions (**Fig. 1d-h, Extended data Fig. 4c-h**). This OMVs-dependent secretion was conserved across all tested CREC sequence types isolated from our cohort (**Extended data Fig. 4h**).

We then tested whether these NDM-loaded OMVs could protect susceptible bacteria from carbapenems. Similar to a free recombinant NDM-5 control, adding CREC-derived OMVs to susceptible clinical isolates of *E. coli*, *K. pneumoniae*, *Enterobacter cloacae*, *Citrobacter freundii*, and *Proteus mirabilis* substantially increased meropenem MICs (**Fig. 1i**). In time-kill assays, NDM-loaded OMVs shielded these strains from meropenem-induced bactericidal activity, enabling sustained bacterial growth (**Fig. 1j-m**). Direct measurements confirmed that OMVs degraded extracellular meropenem as efficiently as the purified free NDM (**Fig. 1j-m**). Thus, gut-colonizing CREC release active NDM exclusively through OMVs, which degrade local carbapenems and protect otherwise susceptible infecting pathogens.

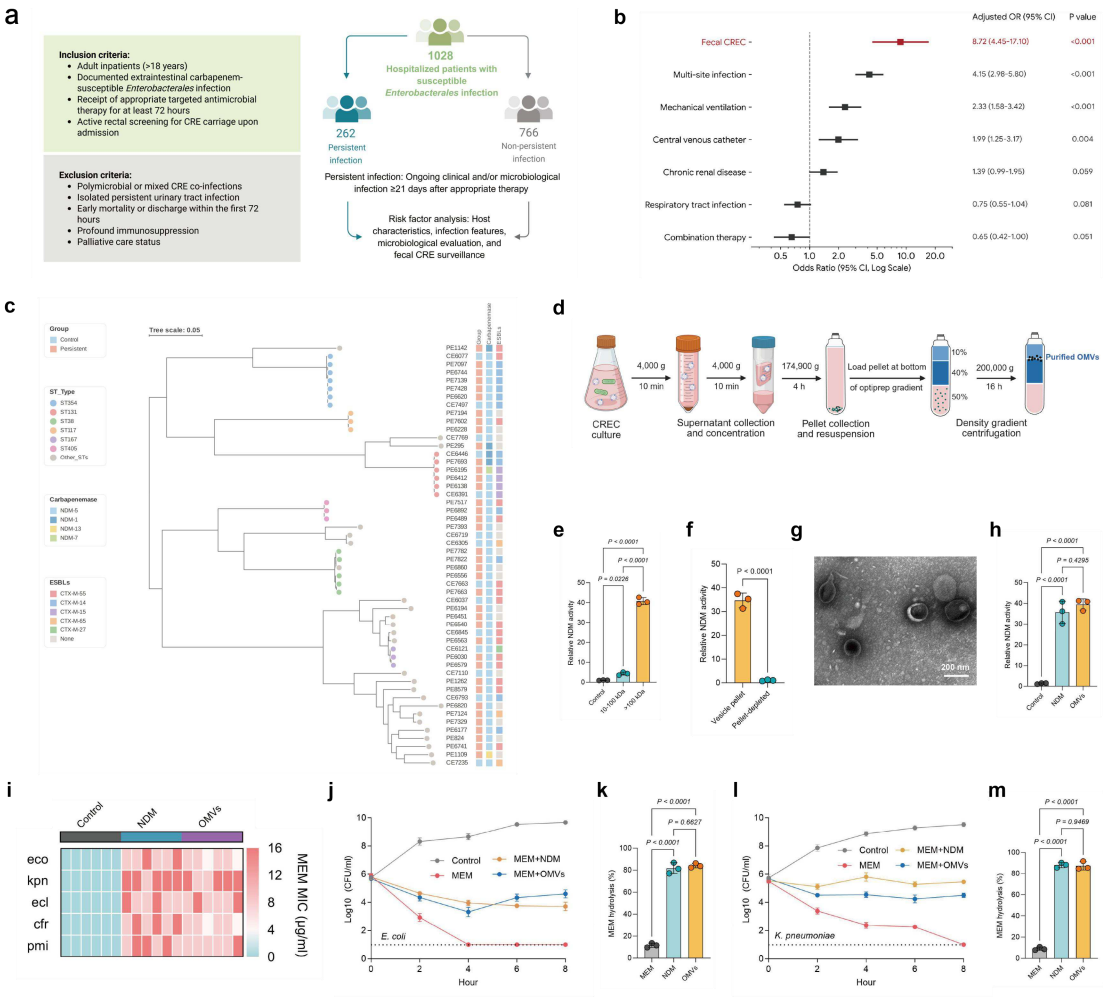


Fig. 1. Fecal CREC colonization is associated with persistent extraintestinal infection and confers OMV-mediated protection in vitro. **a**, Flow diagram detailing the inclusion and exclusion criteria for the clinical cohort, which comprised 1,028 patients with carbapenem-susceptible *Enterobacterales* infections (262 persistent and 766 non-persistent cases). **b**, Multivariate analysis of risk factors for persistent infection. Data show the adjusted odds ratios (OR) and 95% confidence intervals (CI). **c**, Core-genome phylogenetic tree of fecal CREC isolates from the cohort, annotated with sequence types (ST), NDM variants, and extended-spectrum β-lactamase (ESBL) genotypes. **d**, Schematic of the density-gradient ultracentrifugation workflow used to isolate and purify outer membrane vesicles (OMVs) from CREC cultures. **e**, **f**, Relative NDM carbapenemase activity across fractionated CREC cultures, demonstrating that enzymatic

activity partitions strictly with the >100 kDa fraction (**e**) and the vesicle pellet rather than the vesicle-depleted supernatant (**f**). **g**, Representative transmission electron microscopy image of purified CREC OMVs. Scale bar, 100 nm. **h**, Relative carbapenemase activity of the control, purified free NDM, and density-gradient-purified OMVs. **i**, Heatmap showing meropenem (MEM) minimum inhibitory concentrations (MICs) for carbapenem-susceptible clinical isolates (*E. coli* [eco], *K. pneumoniae* [kpn], *E. cloacae* [ecl], *C. freundii* [cfr], and *P. mirabilis* [pmi]) in the presence of control, free NDM, or NDM-loaded OMVs. **j**, **l**, Time-kill curves for carbapenem-susceptible *E. coli* (**j**) and *K. pneumoniae* (**l**) treated with meropenem alone or combined with free NDM or NDM-loaded OMVs. **k**, **m**, Meropenem hydrolysis percentages measured during the respective time-kill assays for *E. coli* (**k**) and *K. pneumoniae* (**m**). All error bars represent standard deviation (SD). Statistical significance was determined by unpaired two-tailed t-tests (**f**), or one-way ANOVA with appropriate post-tests (**e**, **h**, **k**, **m**).

NDM-loaded OMVs impair *in vivo* carbapenem efficacy by accelerating drug degradation

We established a mouse intra-abdominal infection model using carbapenem-susceptible *K. pneumoniae* to evaluate *in vivo* OMVs-mediated protection (**Fig. 2a**). Meropenem treatment alone significantly improved survival and reduced bacterial burdens in the liver and spleen. Co-administration of NDM-loaded OMVs abolished these therapeutic effects, resulting in high mortality and severe organ bacterial loads comparable to untreated controls (**Fig. 2b-d**). In contrast, administering purified free NDM-5 did not impair meropenem efficacy, indicating that the free enzyme lacks sufficient *in vivo* activity to compromise treatment.

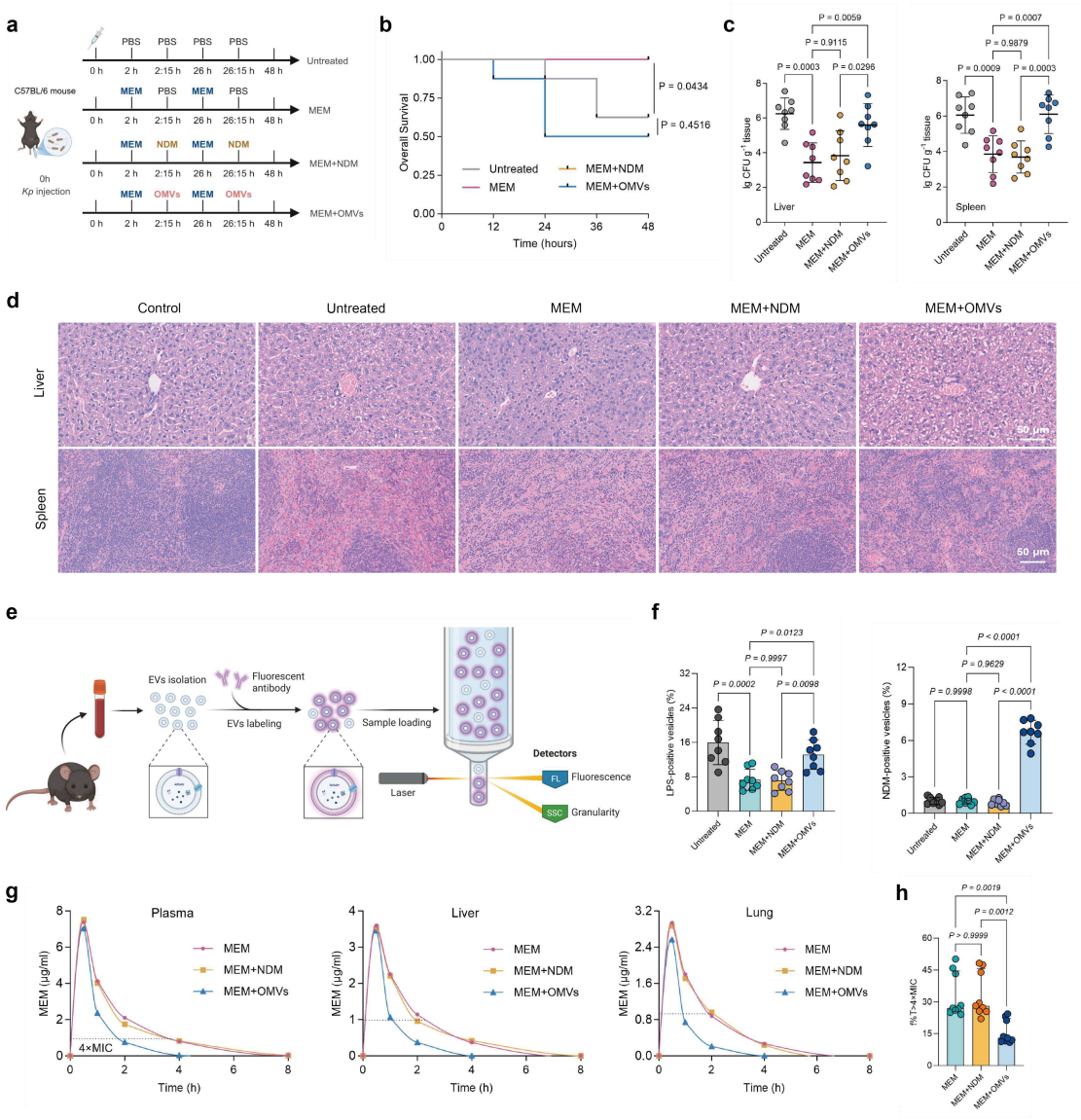
Histopathological analysis mirrored these outcomes: tissues from untreated mice and those receiving meropenem plus OMVs exhibited extensive inflammatory infiltration, multifocal necrosis, and disrupted architecture, whereas tissues from mice treated with meropenem alone or meropenem plus free NDM-5 were largely preserved (**Fig. 2e**).

To track circulating OMVs, we set up a single-vesicle nano-flow cytometry assay using antibodies against lipopolysaccharide (LPS) and NDM, since we confirmed that NDM is localized both inside the lumen and exposed on the vesicle surface via immuno-electron microscopy and hydrolysis assays (**Extended data Fig. 5a-h**). LPS-positive extracellular vesicles were present in all mice and peaked in the untreated and OMVs-treated groups (**Fig. 2e, f**). However, NDM-positive vesicles were found exclusively in mice administered NDM-loaded OMVs, representing roughly 7% of their total circulating vesicle pool (**Fig. 2e, f**). Ex vivo plasma incubation revealed that free NDM-5 rapidly lost its hydrolytic activity and immunodetection signal in mouse plasma, whereas OMV-associated NDM-5 remained remarkably stable and active (**Extended data Fig. 5i, j**). Therefore, vesicle packaging protects NDM from plasma-mediated degradation, preserving its systemic carbapenemase activity.

We next evaluated how this circulating enzyme activity altered drug pharmacokinetics. Meropenem concentrations in the plasma, liver, and lung declined significantly faster in mice receiving NDM-loaded OMVs compared to those receiving meropenem alone or meropenem plus free NDM-5 (**Fig. 2g**). Consequently, the critical pharmacokinetic parameter for efficacy, the fraction of the dosing interval

where free meropenem remains above four times the minimum inhibitory concentration (f%T > 4×MIC)[18], collapsed in the OMVs-treated group (**Fig. 2h**). This confirms that circulating NDM-loaded OMVs actively accelerate *in vivo* meropenem degradation, dropping effective drug exposure below therapeutic thresholds.

Finally, we ruled out horizontal gene transfer as an alternative mechanism of protection. Although bla_{NDM} gene was detectable by PCR in purified OMVs, incubating OMVs with susceptible bacteria failed to produce meropenem-resistant transformants *in vitro*, whereas standard conjugation readily transferred the resistance plasmid (**Extended data Fig. 6a-d**). Crucially, surviving *K. pneumoniae* recovered from the organs of the meropenem-plus-OMVs mouse group failed to grow on meropenem-supplemented agar, confirming the bacteria remained phenotypically susceptible to the antibiotic (**Extended data Fig. 6e**). Together, these findings establish that circulating OMVs protect systemic pathogens strictly through extracellular drug hydrolysis, not by transferring genetic resistance.



188

189 **Fig. 2. NDM-loaded OMVs impair *in vivo* carbapenem efficacy by accelerating drug**

190 **degradation**. **a**, Schematic of the mouse intra-abdominal infection model using a

191 carbapenem-susceptible *Klebsiella pneumoniae* isolate and the corresponding treatment regimens:

192 untreated (PBS), meropenem alone (MEM), MEM with free NDM, or MEM with NDM-loaded

193 OMVs. **b**, Kaplan-Meier overall survival curves for the infected mice over a 48-hour period. **c**,

194 Bacterial burdens recovered from the liver and spleen of mice at 48 hours post-infection. **d**,

195 Representative hematoxylin and eosin (H&E) stained tissue sections of the liver (top row) and

196 spleen (bottom row) showing inflammatory infiltration and tissue architecture across the treatment

groups. Scale bars, 50 μm. **e**, Schematic workflow of the nano-flow cytometry assay used to detect and quantify circulating extracellular vesicles from mouse plasma. **f**, Nano-flow cytometry quantification showing the percentage of circulating LPS-positive and NDM-positive extracellular vesicles in mouse plasma. **g**, Pharmacokinetic profiles tracking meropenem concentrations in the plasma, liver, and lung over an 8-hour window. Dashed horizontal lines indicate four times the minimum inhibitory concentration (4×MIC) of the infecting pathogen. Profiles were calculated using an 8-hour dosing interval to model standard clinical regimens. **h**, The fraction of the dosing interval where free meropenem concentrations remained above the therapeutic target (f%T > 4×MIC) across different treatment groups. Data points represent individual mice. Error bars denote the standard deviation (SD), except in **h**, where they represent the interquartile range (IQR). Statistical significance was determined using one-way ANOVA with Tukey's post hoc test (**c**, **f**), or the Kruskal-Wallis test with Dunn's post hoc test (**h**).

Intestinal barrier disruption promotes systemic translocation of NDM-loaded OMVs and reduces meropenem exposure

We next investigated how gut-derived OMVs reach the systemic circulation. Using a Caco-2 Transwell model, we found that dextran sulfate sodium (DSS)-induced disruption of epithelial tight junctions, which was indicated by reduced ZO-1 staining, dose-dependently increased OMVs translocation into the basolateral compartment (**Extended data Fig. 7a-c**). To track this process *in vivo*, we orally administered fluorescent OMVs derived from an OmpF-mCherry CREC reporter strain to mice with or without DSS-induced intestinal injury (**Extended data Fig. 7d, e**). While control mice restricted OMVs dissemination, DSS treatment, which caused

pronounced colonic shortening and mucosal damage, dramatically increased mCherry fluorescence in extraintestinal organs including the liver, lung, kidney, and ovary (**Extended data Fig. 7f-h**). This indicates that mucosal barrier injury directly facilitates the systemic translocation of luminal OMVs.

To determine how this barrier injury affects systemic antibiotic exposure, we evaluated a mouse model combining intestinal CREC colonization with DSS-induced colitis (**Fig. 3a**). Mice were colonized with wild-type CREC or an isogenic Δ*bla*$_{NDM}$ mutant for 14 days, administered DSS during the second week, and then given a single intravenous dose of meropenem. Fecal plating confirmed stable gut colonization across groups (**Fig. 3b**). Although DSS caused significant local colonic injury (**Fig. 3c, e**), plasma procalcitonin (PCT) levels remained baseline and blood cultures were negative, ruling out overt bacteremia or systemic inflammation as confounding factors (**Fig. 3d, f**). Using nano-flow cytometry, we observed an overall increase in circulating LPS-positive vesicles following DSS exposure; however, NDM-positive vesicles specifically accumulated only in mice both colonized with wild-type CREC and subjected to DSS (**Fig. 3g, h**). Consequently, meropenem concentrations in the plasma, liver, and lung declined more rapidly in the CREC-plus-DSS group compared to controls, severely compressing the critical pharmacokinetic parameter for efficacy, the fraction of the dosing interval where free meropenem remains above four times the minimum inhibitory concentration (f%T > 4×MIC) (**Fig. 3i, j**). Crucially, this accelerated drug clearance was absent in mice colonized with the Δ*bla*$_{NDM}$ mutant, confirming that the systemic pharmacokinetic

241 failure relies strictly on translocated NDM-loaded OMVs.

242 We found parallel evidence for this gut-to-blood translocation in our human
243 cohort. Hospitalized patients with intestinal CREC colonization harbored a
244 significantly higher proportion of circulating NDM-positive vesicles than
245 non-colonized controls, despite maintaining similar overall levels of LPS-positive
246 vesicles (**Fig. 3k, l**). Furthermore, the abundance of circulating NDM-positive
247 vesicles correlated positively with plasma zonulin, a proposed marker of intestinal
248 permeability[19] (**Fig. 3m**). Retrospective analysis of patient records confirmed that
249 intestinal CREC carriers frequently presented with clinical conditions known to
250 compromise mucosal barrier integrity, such as chemotherapy[20], radiotherapy[21], recent
251 broad-spectrum antibiotic use[22], and aging[23] (**Extended data Table 1**). Together, these
252 results demonstrate that intestinal barrier injury enables NDM-loaded OMVs from
253 gut-colonizing CREC to infiltrate the bloodstream, where they act as a systemic drug
254 sink that undermines carbapenem therapy at distant infection sites.

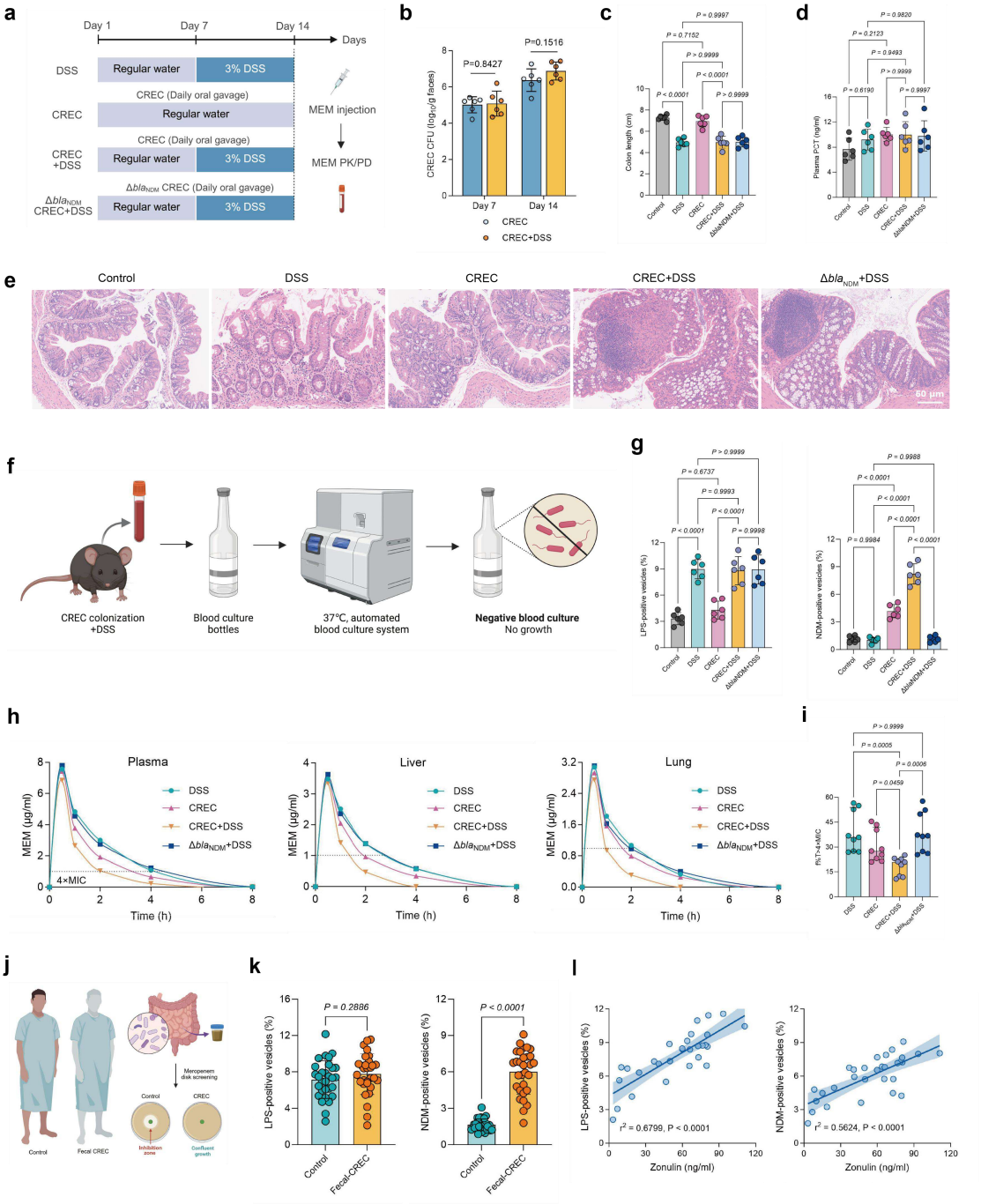


Figure 3. **Intestinal barrier disruption facilitates the systemic translocation of NDM-loaded OMVs and reduces therapeutic carbapenem exposure**. **a**, Experimental timeline for the mouse model combining intestinal CREC (or isogenic Δ*bla*$_{NDM}$) colonization, DSS-induced colitis, and meropenem (MEM) administration. **b**, Fecal CREC bacterial burdens on days 7 and 14 confirming stable intestinal colonization across groups. **c**, **e**, Colon length (c) and representative hematoxylin

and eosin (H&E) stained colon sections (e) demonstrating local mucosal tissue injury following DSS exposure. Scale bar, 50 μm. **d**, **f**, Plasma procalcitonin (PCT) levels (**d**) and schematic of blood culture results (**f**) confirming the absence of systemic inflammation or overt bacteremia. **g**, Nano-flow cytometry quantification of circulating LPS-positive and NDM-positive extracellular vesicles in mouse plasma. **h**, Pharmacokinetic profiles tracking meropenem concentrations in the plasma, liver, and lung. Dashed horizontal lines indicate four times the minimum inhibitory concentration (4×MIC) of the infecting pathogen referenced in Fig. 2, and 0.25 μg/mL, which is the most common meropenem MIC for carbapenem-susceptible *Enterobacterales* in our cohort. Profiles were calculated using an 8-hour dosing interval to model standard clinical regimens. **i**, The fraction of the dosing interval where free meropenem remains above four times the minimum inhibitory concentration (f%T > 4×MIC) across the mouse treatment groups. **j**, Schematic outlining the analysis of circulating plasma vesicles in hospitalized patients with or without intestinal CREC colonization. **k**, Proportion of circulating LPS-positive and NDM-positive extracellular vesicles in the plasma of these hospitalized patients. **l**, Correlations between plasma zonulin levels (a biomarker of intestinal permeability) and circulating vesicle abundance in human patients. Associations were assessed using Pearson correlation analysis. The effect size, represented by Pearson's correlation coefficient (r) was calculated from the coefficient of determination (r^2) derived via simple linear regression. Plotted data points represent individual mice or human patients, with error bars showing the standard deviation (SD), except in **i**, where they represent the interquartile range (IQR). Statistical significance was determined using unpaired two-tailed t-tests (**b**, **k**), one-way ANOVA with Tukey's post hoc test (**c**, **d**, **g**), or the Kruskal-Wallis test with Dunn's post hoc test (**i**).

Porin-mediated antibiotic entry determines the protective activity of carbapenemase-loaded OMVs

To understand how NDM-loaded OMVs could protect the susceptible bacteria, we first tested whether these vesicles transfer functional NDM directly to recipient cells. We incubated carbapenem-susceptible *E. coli* and *K. pneumoniae* with NDM-loaded OMVs for up to 8 h. After removing the OMVs, the meropenem MICs of the recipient cells remained unchanged (**Fig. 4a-c**). This indicates that the OMVs protect susceptible strains strictly through extracellular meropenem hydrolysis, rather than by conferring sustained resistance via enzyme transfer.

For luminal NDM to hydrolyze meropenem, the antibiotic must cross the vesicle membrane. In *E. coli*, OmpC and OmpF are the primary outer membrane porins facilitating carbapenem entry[24,25]. To determine if they function similarly in OMVs, we generated single (Δ*ompC*, Δ*ompF*) and double (Δ*ompC*Δ*ompF*) deletion mutants in the CREC background (**Fig. 4d-f**). SDS-PAGE confirmed the loss of these porins (**Fig. 4e, f**), while nanoparticle tracking analysis showed that the deletions did not alter total OMVs production (**Fig. 4g**).

Detergent disruption of equal numbers of OMVs with Triton X-100 revealed comparable total NDM activity across all four strains, confirming that porin loss does not affect the amount of active NDM packaged into vesicles (**Fig. 4h**). However, intact OMVs from the Δ*ompC* and Δ*ompF* mutants showed significantly reduced hydrolytic activity compared to wild-type OMVs, with a further reduction observed in the double mutant (**Fig. 4h**). Consequently, while wild-type OMVs increased

meropenem MICs by 64- to 128-fold in susceptible *E. coli* and *K. pneumoniae*, OMVs from single mutants provided only a 16- to 32-fold increase, and the double mutant yielded just a 2- to 4-fold increase relative to the no-OMVs control (**Fig. 4i**).

To directly measure antibiotic entry, we incubated OMVs derived from the bla_{NDM}-knockout CREC strain with meropenem and quantified drug concentrations in both the isolated vesicle fraction and the surrounding supernatant (**Fig. 4j**). Meropenem accumulation within OMVs progressively decreased with sequential porin deletion, reaching its lowest level in vesicles from the $\Delta ompC \Delta ompF$ strain (**Fig. 4k**). Conversely, meropenem concentrations in the supernatant exhibited the opposite trend: the lowest levels were observed after incubation with wild-type OMVs, while the highest levels remained after incubation with double-knockout OMVs. Consistent with this structural barrier, deleting both porins increased the meropenem MIC of the parent CREC strain four-fold (**Fig. 4l**). Together, these data demonstrate that OmpC and OmpF are required for meropenem to access intra-vesicular NDM, dictating the protective efficacy of OMVs.

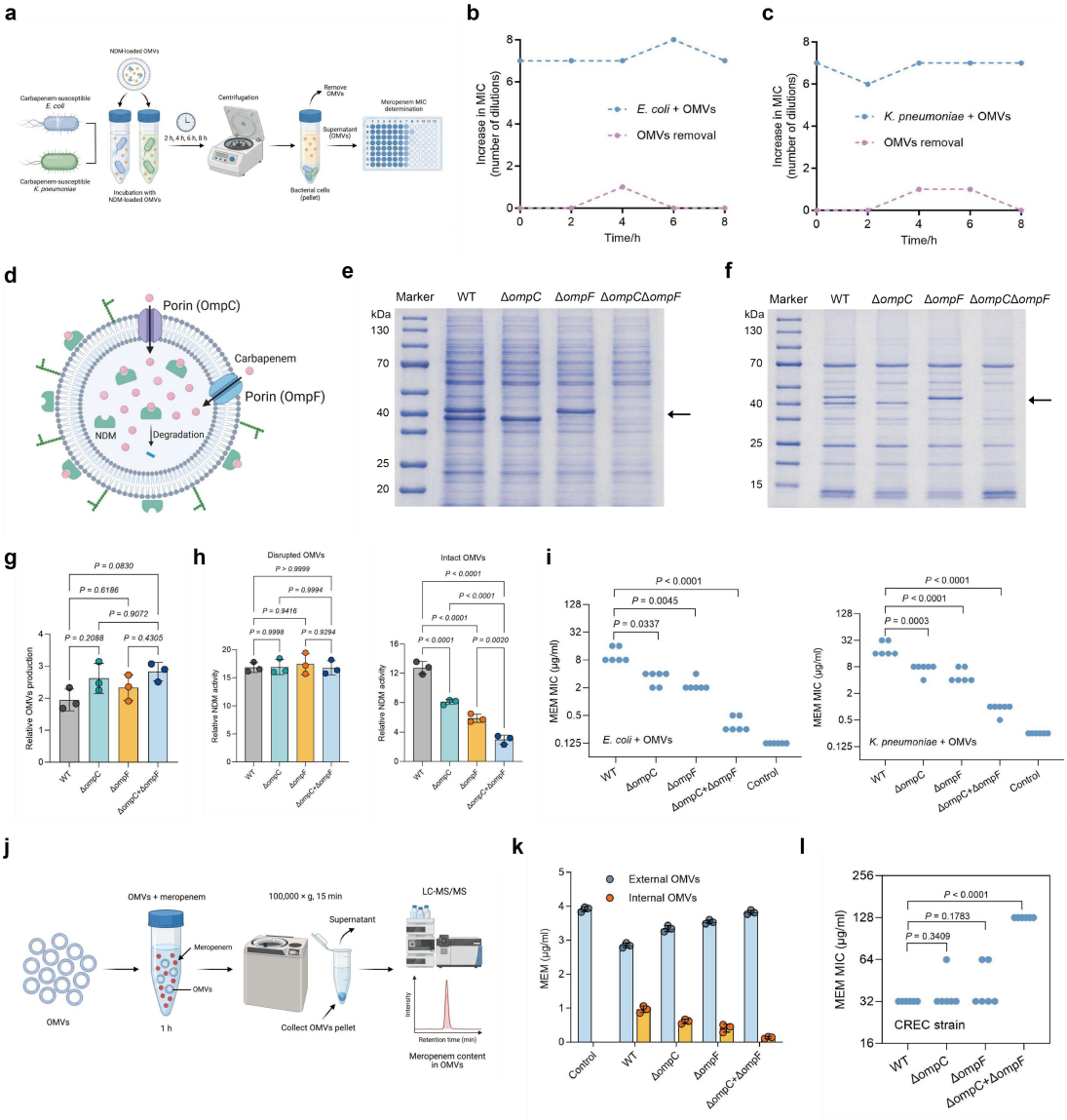


Figure 4. Porin-mediated antibiotic entry dictates the protective activity of carbapenemase-loaded OMVs. **a**, Experimental workflow testing whether NDM-loaded OMVs transfer functional resistance to recipient cells. Carbapenem-susceptible *E. coli* and *K. pneumoniae* were incubated with OMVs for up to 8 hours, followed by OMVs removal and determination of recipient meropenem (MEM) MICs. **b**, **c**, Fold-increase in meropenem MICs for *E. coli* (b) and *K. pneumoniae* (c) in the continuous presence of OMVs versus after OMVs removal. **d**, Schematic illustrating that extracellular meropenem must cross the vesicle membrane via OmpC and OmpF porins to be hydrolyzed by luminal NDM. **e**, **f**, SDS-PAGE analysis of

bacterial strains (e) and purified OMVs (f) from the wild-type (WT) CREC parent, single porin knockouts (Δ*ompC*, Δ*ompF*), and the double knockout (Δ*ompC*Δ*ompF*). Arrows indicate the major porin bands (~35-40 kDa). **g**, Relative OMVs production across the four CREC strains, quantified by nanoparticle tracking analysis. **h**, Relative NDM carbapenemase activity of the four OMVs types following Triton X-100 disruption (left) compared to intact, untreated OMVs (right). **i**, Meropenem MICs for susceptible *E. coli* (left) and *K. pneumoniae* (right) when incubated with OMVs derived from the WT or porin-deficient CREC strains. **j**, Schematic for measuring direct antibiotic entry into OMVs. OMVs from the bla_{NDM}-knockout CREC backgrounds were incubated with meropenem for 1 hour, ultracentrifuged, and meropenem content was quantified by LC-MS/MS. **k**, Meropenem concentrations recovered from the OMVs pellet (internal) and the surrounding supernatant (external) after the 1-hour incubation. **l**, Meropenem MICs of the parent CREC strain and the corresponding porin-deficient mutants. Error bars show the standard deviation (SD). Statistical significance was determined using one-way ANOVA with Tukey's post hoc test.

This porin dependency explains a clinical discrepancy in our cohort: unlike CREC, intestinal colonization with carbapenem-resistant *K. pneumoniae* (CRKP) was not associated with persistent extraintestinal infection (**Extended Data Table 1**). Whole-genome sequencing showed that our CRKP population was predominantly sequence type 11 (ST11) (**Extended Data Fig. 8a**). Nearly all ST11 isolates carried $bla_{\text{KPC-2}}$, which encodes a soluble periplasmic carbapenemase[26]. Western blotting and hydrolysis assays confirmed that functional KPC-2 was mostly confined to the OMVs

lumen, as intact vesicles showed little activity until disrupted by detergent (**Extended Data Fig. 8e-h**). Furthermore, the ST11 CRKP isolates harbored a frameshift mutation truncating OmpK35, alongside an Asp-Gly (DG) insertion in the OmpK36 channel known to restrict carbapenem entry[27] (**Extended Data Fig. 8a-d**). Therefore, the dominant ST11 clone packages a luminal carbapenemase within OMVs that have severely restricted permeability.

To verify this, we constructed an isogenic OmpK36-revertant strain lacking the DG insertion (WT-ΔDG). OMVs from this revertant increased the meropenem MICs of susceptible strains by approximately 16-fold, whereas OMVs from the wild-type ST11 parent provided only a 2- to 4-fold increase (**Extended Data Fig. 8j**). Predictably, the parent strain itself had a four-fold higher meropenem MIC than the revertant (**Extended Data Fig. 8k**). In time-kill assays, OMVs from the wild-type ST11 strain offered little protection, whereas OMVs from the OmpK36-revertant strongly reduced the meropenem-mediated killing of susceptible bacteria (**Extended Data Fig. 8l**). Direct measurements confirmed that the revertant OMVs hydrolyzed substantially more meropenem than the wild-type OMVs (**Extended Data Fig. 8m**). Ex vivo plasma incubation revealed that while free KPC-2 in the supernatant (10-100 kDa) rapidly lost its hydrolytic activity in mouse plasma, OMVs-associated KPC-2 (>100 kDa) from the OmpK36-revertant strain remained remarkably stable and active (**Extended Data Fig. 8n**). Thus, vesicle packaging protects KPC from plasma-mediated degradation, preserving its systemic carbapenemase activity.

Ultimately, the protective capacity of carbapenemase-loaded OMVs depends on

both the specific enzyme they carry and the vesicle's permeability to antibiotics. While *E. coli* OmpC and OmpF allow meropenem to reach vesicle-bound NDM, the dominant ST11 CRKP clone features porin defects that restrict antibiotic access to luminal KPC-2. Thus, enzyme localization and porin architecture jointly determine whether gut-derived vesicles can neutralize systemic carbapenems.

Meropenem exposure increases OMVs production and vesicle-associated NDM activity

Because antibiotic stress can profoundly alter bacterial physiology, we tested whether meropenem exposure dynamically modulates this OMVs-mediated protective effect. Quantitative proteomics of OMVs derived from CREC cultured with or without meropenem (4 μg/mL) identified over 1,000 protein features (**Fig. 5a, b**). NDM was heavily enriched in OMVs from meropenem-exposed cultures, exhibiting an approximately 12-fold increase compared to untreated controls (**Fig. 5c, d**). Accordingly, these meropenem-induced OMVs displayed a 15-fold higher carbapenemase activity (**Fig. 5e**). This induction is driven specifically by cell-wall stress. Nanoparticle tracking analysis confirmed that exposure to β-lactams (meropenem, piperacillin-tazobactam, and ceftazidime) significantly stimulated overall OMVs production, whereas non-β-lactam antibiotics (amikacin and ciprofloxacin) did not alter vesicle yield (**Fig. 5f**).

To define the genetic basis for this enhanced NDM production, we tracked plasmid and transcript dynamics during antibiotic exposure. Meropenem significantly increased both the copy number of the *bla*$_{NDM}$-carrying plasmid and the direct

transcription of *bla*$_{NDM}$ (**Fig. 5g**). Furthermore, meropenem upregulated *secA* (a component of the Sec-dependent export pathway) and *lspA* (signal peptidase II, required for lipoprotein maturation)[28], while leaving the expression of the signal peptidase I gene *lepB* unchanged (**Fig. 5h**). This targeted transcriptional response perfectly supports the accelerated biogenesis, processing, and membrane targeting of NDM, a lipidated protein strictly dependent on signal peptidase II.

Ultimately, meropenem triggers a feed-forward protective response in intestinal CREC. The antibiotic simultaneously stimulates global OMVs release and hyper-loads these escaping vesicles with functional NDM (**Fig. 5i**). This stress-induced surge in vesicle-associated carbapenemase activity acts to further accelerate systemic meropenem degradation, heavily compounding the loss of effective antibiotic exposure.

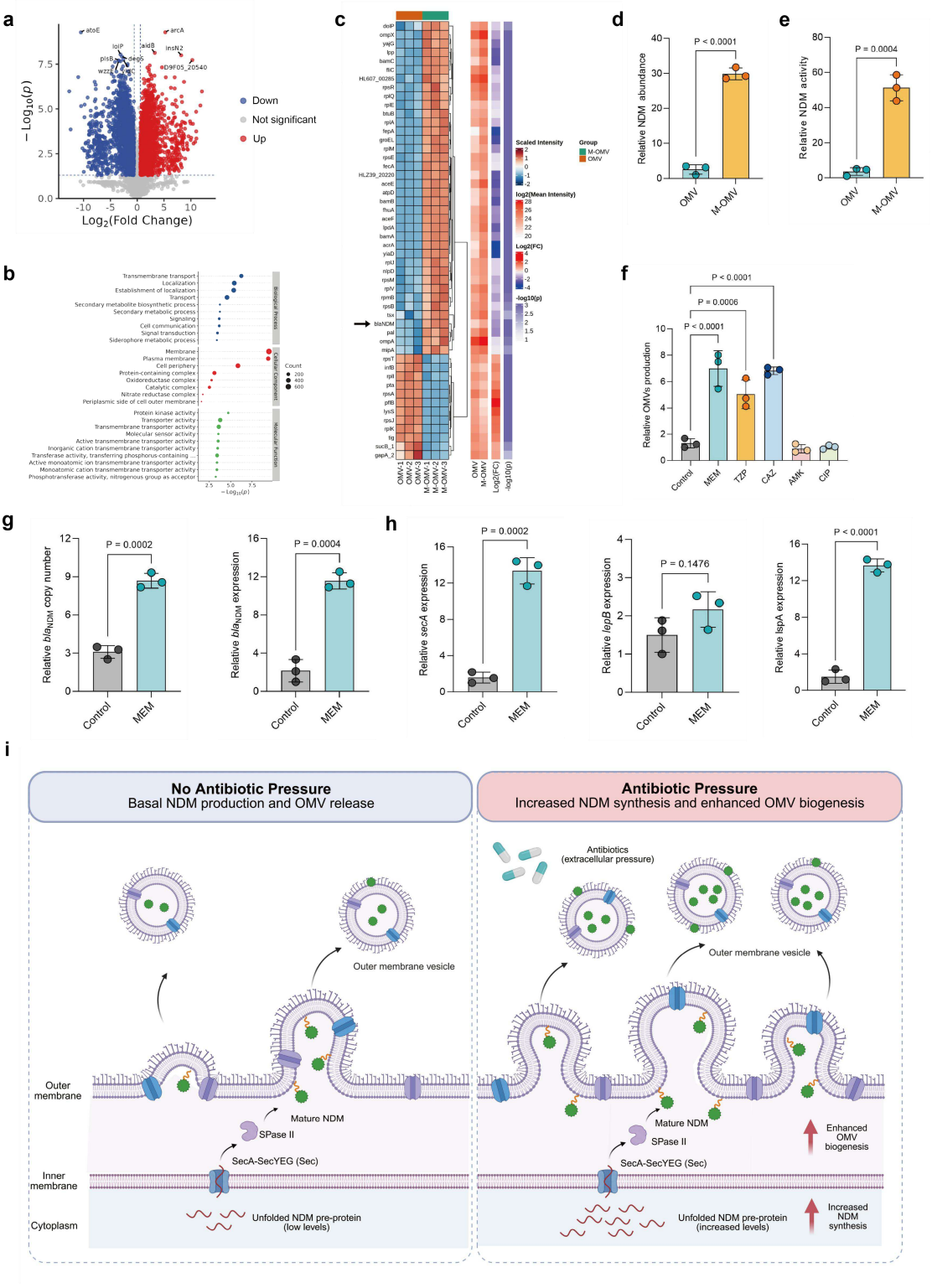


Figure 5. **Meropenem exposure stimulates OMV release and enriches vesicle-associated NDM activity**. **a**, **b**, Quantitative proteomic analysis of OMVs isolated from CREC cultured with or without meropenem (MEM). The volcano plot (a) and enrichment analysis (b) display

differentially abundant proteins in the OMVs proteome following antibiotic stress. **c**, Heatmap of differentially abundant proteins comparing OMVs from untreated (OMV) and meropenem-treated (M-OMV) cultures. The black arrow highlights the enrichment of NDM. **d**, **e**, Relative NDM protein abundance (d) and corresponding vesicle-associated carbapenemase activity (e) in OMVs derived from untreated versus meropenem-exposed cultures. **f**, Relative OMVs production measured by nanoparticle tracking analysis after bacterial exposure to β-lactams (meropenem [MEM], piperacillin-tazobactam [TZP], ceftazidime [CAZ]) or non-β-lactams (amikacin [AMK], ciprofloxacin [CIP]). **g**, Relative bla_{NDM} plasmid copy number (left) and bla_{NDM} transcript expression (right) following meropenem exposure. **h**, Relative mRNA expression of the Sec export pathway motor (*secA*) and signal peptidases (*lepB*, *lspA*) with and without meropenem treatment. Meropenem specifically upregulates *secA* and *lspA* (signal peptidase II), which are required for lipoprotein maturation. **i**, Schematic of the feed-forward model. Extracellular antibiotic pressure stimulates CREC to increase NDM synthesis, upregulate lipoprotein processing, and enhance the biogenesis of OMVs hyper-loaded with functional NDM. Plotted data points represent independent biological replicates, with error bars showing the standard deviation (SD). Statistical significance was determined using unpaired two-tailed t-tests (**d**, **e**, **g**, **h**) or one-way ANOVA with Tukey's post hoc test (**f**).

NDM-stable and non-β-lactam regimens retain efficacy despite circulating NDM-loaded OMVs

Because clinical guidelines do not recommend decolonizing intestinal CRE[29,30], we tested alternative antibiotics designed to bypass this OMVs-mediated drug sink. *E. coli* and *K. pneumoniae* isolates from persistent infections in our cohort remained

433 highly susceptible to amikacin (>93%) and aztreonam-avibactam (100%) (**Fig. 6a**).
434 Hydrolysis assays confirmed that NDM-loaded OMVs could not degrade either drug
435 (**Fig. 6b**). Aztreonam resists metallo-β-lactamase cleavage, and avibactam neutralizes
436 co-produced serine β-lactamase[31].

437 To test these alternatives *in vivo*, we adapted our CREC-colonization and
438 DSS-colitis model to include a secondary *K. pneumoniae* pneumonia. Following
439 intestinal colonization and barrier disruption, mice were intranasally challenged with
440 a carbapenem-susceptible *K. pneumoniae* strain and treated with PBS, meropenem,
441 amikacin, or aztreonam-avibactam (**Fig. 6c**). Although survival rates were similar
442 across groups over the initial 48-hour window, aztreonam-avibactam substantially
443 reduced lung bacterial burdens compared to untreated controls, whereas meropenem
444 failed to clear the pulmonary infection (**Fig. 6d**). Histopathology confirmed these
445 outcomes: aztreonam-avibactam prevented alveolar wall thickening, inflammatory
446 infiltration, and structural tissue injury. Meropenem-treated lungs remained as
447 damaged as untreated controls (**Fig. 6f**). Systemically, both amikacin and
448 aztreonam-avibactam effectively reduced blood bacterial counts and lowered plasma
449 procalcitonin levels (**Fig. 6d, e**).

450 Tracking circulating vesicles post-treatment showed that only amikacin reduced
451 total plasma LPS-positive vesicle abundance. In contrast, the proportion of
452 NDM-positive vesicles surged in mice treated with meropenem or
453 aztreonam-avibactam, though this increase only reached statistical significance in the
454 meropenem group (**Fig. 6g**). This indicates that systemic β-lactam exposure

selectively enriches the NDM cargo of circulating vesicles without increasing overall vesicle output. Despite this increase in circulating NDM, aztreonam concentrations in the plasma and lung remained stable. Meropenem, however, was rapidly degraded, severely compressing its therapeutic window (f%T > 4 × MIC) (**Fig. 6h**). Amikacin pharmacokinetics showed a high Cmax/MIC ratio in the plasma but limited lung penetration (**Fig. 6i**), which explains its efficacy in clearing bacteremia without resolving the primary pneumonia.

Ultimately, these data confirm that alternative antimicrobial therapies can successfully bypass the gut-derived OMV drug sink. NDM-stable β-lactam combinations (aztreonam-avibactam) and non-β-lactam (amikacin) retain potent in vivo efficacy against susceptible infections despite intestinal CREC colonization, offering a directed therapeutic strategy for patients at high risk of meropenem failure.

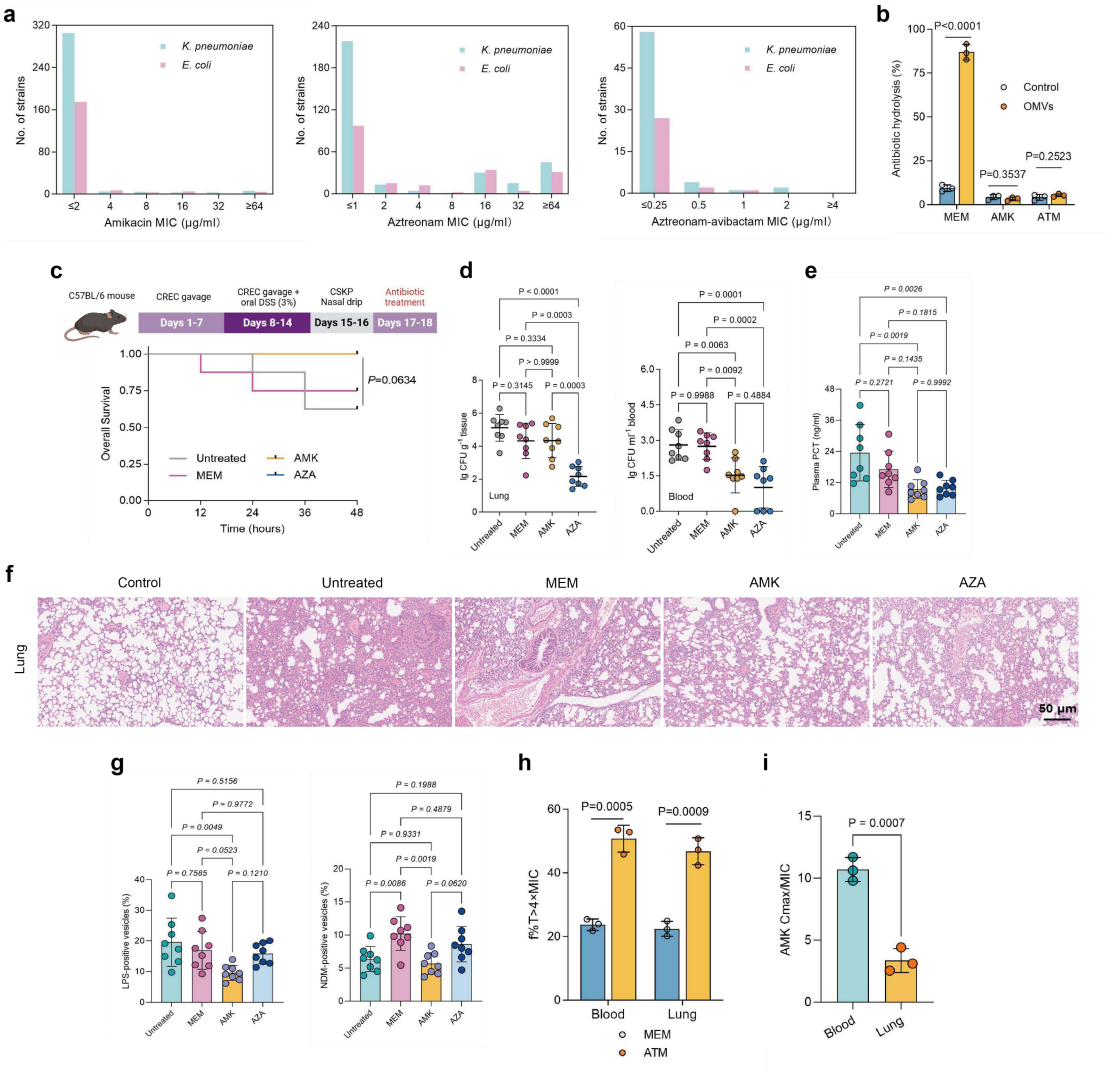


Figure 6. NDM-stable and non-β-lactam regimens retain in vivo efficacy despite circulating NDM-loaded OMVs. a, Minimum inhibitory concentration (MIC) distributions of amikacin, aztreonam, and aztreonam-avibactam for carbapenem-susceptible *K. pneumoniae* and *E. coli* clinical isolates recovered from patients with persistent infections. **b**, Percentage of antibiotic hydrolysis for meropenem (MEM), amikacin (AMK), and aztreonam (ATM) following in vitro incubation with control buffer or purified NDM-loaded OMVs. **c**, Experimental timeline for the secondary pneumonia mouse model (top) and Kaplan-Meier overall survival curves (bottom) comparing untreated mice to those treated with meropenem (MEM), amikacin (AMK), or aztreonam-avibactam (AZA). **d**, **e**, Bacterial burdens recovered from the lung and blood (d),

alongside plasma procalcitonin (PCT) levels (e) at 48 hours post-infection across the treatment groups. **f**, Representative hematoxylin and eosin (H&E)-stained lung tissue sections showing alveolar architecture, wall thickening, and inflammatory infiltration across the experimental groups. Scale bar, 50 μm. **g**, Nano-flow cytometry quantification of circulating LPS-positive (left) and NDM-positive (right) extracellular vesicles in mouse plasma following the indicated treatments. **h**, The fraction of the dosing interval where free meropenem (MEM) or aztreonam (ATM) concentrations remained above the therapeutic target (f%T > 4×MIC) in the blood and lung. **i**, The ratio of maximum plasma concentration to MIC of the infecting pathogen (Cmax/MIC) for amikacin (AMK) in the blood and lung. Plotted data points represent independent samples or individual mice, with error bars showing the standard deviation (SD). Statistical significance was determined using unpaired two-tailed t-test (**b**, **h**, **i**), one-way ANOVA with Tukey's post hoc test (**d**, **e**, **g**).

Discussion

Persistent infection despite appropriate antimicrobial therapy remains difficult to explain when the infecting pathogen is susceptible by standard antimicrobial susceptibility testing (AST). In this study, intestinal colonization with NDM-producing carbapenem-resistant *Escherichia coli* (CREC) is independently associated with persistent extraintestinal infection caused by carbapenem-susceptible *Enterobacterales*. Following intestinal barrier injury, CREC-derived NDM-loaded outer membrane vesicles (OMVs) translocate into the circulation, accelerate carbapenem degradation and reduce effective systemic drug exposure. Consequently, this circulating resistance mechanism impairs the treatment of susceptible infections

499 at distant sites, without requiring the infecting pathogen to acquire resistance. These
500 findings indicate that the gut resistome can actively compromise antibiotic efficacy
501 beyond the local site of colonization.

502 Previous studies have shown that β-lactamase-containing OMVs can degrade
503 antibiotics and protect susceptible bacteria[11,14]. A recent study detected circulating
504 carbapenemase-containing OMVs in patients with intestinal CRE colonization and
505 showed that these vesicles retain antibiotic-degrading activity[32]. Our findings extend
506 these observations by linking intestinal CREC colonization to persistent
507 extraintestinal infection in a clinical cohort and mechanistically proving how
508 NDM-loaded OMVs deplete systemic antibiotic levels. By combining epithelial
509 translocation assays, *in vivo* OMVs tracking, single-vesicle plasma profiling, and
510 pharmacokinetic modeling, we defined a complete gut-to-bloodstream pathway that
511 drives clinical treatment failure. The primary advance of our work is demonstrating
512 that a resistant colonizer residing in one anatomical compartment can lower systemic
513 drug exposure enough to rescue an unrelated, susceptible pathogen elsewhere in the
514 host.

515 Intestinal barrier integrity dictates whether this resistance activity remains
516 localized to the gut or becomes systemic. Single-particle studies have detected
517 bacterial extracellular vesicles in human blood and linked circulating vesicle levels to
518 intestinal permeability[16,33]. In our models, epithelial injury increased OMVs
519 translocation and circulating NDM-positive vesicle abundance, causing meropenem to
520 decline more rapidly from the circulation. Carbapenem efficacy relies on maintaining

free drug concentrations above the MIC for a sufficient proportion of the dosing interval[34,35]. Circulating NDM-loaded OMVs reduced meropenem exposure and shortened the fraction of the dosing interval during which free drug concentrations remained above four times the MIC of the infecting pathogen (f%T > 4×MIC). We detected significantly more NDM-positive circulating vesicles in CREC-colonized patients, and these correlated with plasma intestinal barrier injury marker. Indeed, the majority of our CREC-colonized patients had underlying conditions known to damage the gut mucosa, such as chemotherapy[20], radiotherapy[21], recent broad-spectrum antibiotic use[22], and aging[23]. Both the mouse models and the clinical cohort demonstrate that the intestinal mucosal barrier injury establishes a functional balance: it confines colonizing CREC within the intestinal lumen, preventing systemic infection, while allowing the release of CREC-derived NDM-loaded OMVs into the systemic circulation. These findings suggest that NDM-producing gut colonization becomes pharmacologically important when the intestinal barrier is impaired. Therapeutic drug monitoring and the direct detection of circulating carbapenemase-containing vesicles could be explored as complementary approaches to rapidly identify this clinical phenotype.

The ability of carbapenemase-loaded OMVs to degrade antibiotics also depends on the permeability of their membranes. Previous work showed that the major porin OmpC and OmpF facilitate β-lactam entry into *E. coli* OMVs, allowing access to intra-vesicular β-lactamase[24]. In our study, deleting OmpC or OmpF substantially reduced meropenem hydrolysis and OMVs-mediated protection, with the greatest

543 reduction observed when both porins were deleted. Importantly, total functional NDM
544 activity following detergent disruption was equivalent between wild-type and
545 porin-deficient OMVs, confirming that porin loss restricts substrate access rather than
546 reducing NDM packaging. OMVs-mediated hydrolysis, therefore, depends on both
547 the presence of active enzyme and structural substrate access.

548 The CRKP findings further extend this principle. KPC-2 was mainly located
549 within the lumen of CRKP OMVs, whereas the dominant ST11 isolates lacked
550 functional OmpK35 and carried a channel-constricting DG insertion in OmpK36[27].
551 Restoring the wild-type OmpK36 sequence in our ST11 CRKP strain increased
552 meropenem hydrolysis by the OMVs and restored their ability to protect susceptible
553 bacteria. Thus, KPC-containing OMVs are not intrinsically incapable of protecting
554 other bacteria; rather, the porin architecture of the ST11 background structurally limits
555 antibiotic access to luminal KPC-2. Notably, porin defects have opposite
556 consequences for the bacterial cell and the released vesicle: reduced permeability can
557 increase resistance of the bacterium while limiting the ability of its OMVs to
558 hydrolyze extracellular carbapenems.

559 This selective permeability explains why CREC, but not CRKP, colonization was
560 associated with persistent infection in our cohort. ST11 and KPC-2 represent the
561 predominant CRKP lineage and carbapenemase in China[36], and large-scale genomic
562 analyses show that OmpK35 truncation combined with the OmpK36 DG insertion is
563 universally prevalent among Chinese *bla*$_{KPC}$-carrying ST11 CRKP[27,36]. The population
564 structure of CRKP varies across regions, with epidemic lineages such as ST258,

ST307, ST147 and ST231 showing different geographical distributions[37,38]. ST258, the dominant clone in the USA, Greece, Israel, and several South American countries[37,39,40], exhibits ubiquitous OmpK35 truncation and a high prevalence of OmpK36 L3 insertions[27]. While these porin mutations enhance the survival of epidemic CRKP clones against antimicrobial killing[27,41], they simultaneously compromise their capacity to protect susceptible bacteria in the environment via OMVs. Different combinations of clone, carbapenemase, and porin genotype will inherently produce diverse OMVs phenotypes.

Antibiotic exposure can further amplify this OMVs-mediated pathway, as antibiotics are known to stimulate bacterial extracellular vesicle release[42]. In our experiments, β-lactams increased OMVs production, and meropenem markedly increased NDM enrichment and carbapenemase activity in CREC-derived OMVs. Mechanistically, meropenem increased bla_{NDM} plasmid copy number and gene transcription, and specifically upregulated *secA* and signal peptidase II (*lspA*), the exact machinery required to export and lipidate NDM[12,28]. These findings support a feed-forward process where antibiotic pressure stimulates CREC to increase NDM expression and lipoprotein processing, releasing more OMVs packed with higher levels of functional NDM. These vesicles then degrade systemic meropenem at an accelerated rate. Thus, meropenem exposure actively amplifies the very resistance mechanism that undermines treatment.

Our findings may also have direct implications for clinical treatment. Current guidelines do not support routine decolonization of CRE carriers due to limited

evidence of sustained clinical benefit[29,30]. Consequently, the treatment of extraintestinal infections remains focused exclusively on the susceptibility profile of the infecting organism. This study raises significant concern regarding the continued reliance on NDM-labile β-lactam monotherapy in patients with NDM-producing CREC carriage and unexplained persistent infection despite documented pathogen susceptibility. In our mouse models, meropenem failed against susceptible *K. pneumoniae* infection, whereas NDM-stable aztreonam-avibactam and the non-β-lactam amikacin retained efficacy. Because these alternative regimens successfully bypass circulating NDM-loaded OMVs, clinical treatment strategies may need to consider both the infecting pathogen and the gut resistome.

More broadly, our findings expand the clinical definition of antimicrobial resistance beyond the genetic profile of the infecting isolate. Conventional susceptibility testing evaluates pathogens in isolation, inherently failing to capture systemic antibiotic modification by distinct, anatomically separated microbial populations. By demonstrating that the gastrointestinal microbiota functions as a pharmacologically active reservoir, we show that resistant colonizers can actively dictate therapeutic outcomes without causing the primary infection or transferring resistance genes. Ultimately, this study shifts the paradigm of antimicrobial resistance from a localized cellular trait to a remote, microbiome-mediated pharmacokinetic driver of treatment failure, establishing that effective clinical management must account for both the targeted pathogen and the systemic influence of the gut resistome.

Methods

Inclusion and ethics

The research complied with all applicable ethical regulations. The human clinical study was approved by the ethics committee of Renji Hospital, Shanghai Jiao Tong University School of Medicine, Shanghai, China (approval no. LY2024-296). All animal procedures followed the ethical guidelines outlined in the Guide for the Care and Use of Laboratory Animals proposed by the Institute for Laboratory Animal Research of the National Academy of Sciences, and all experimental protocols were approved by the Animal Welfare Committee of Renji Hospital, Shanghai Jiao Tong University School of Medicine, Shanghai, China (approval no. RJ2025-547).

Retrospective cohort and participant selection

We retrospectively analyzed a cohort of hospitalized patients with carbapenem-susceptible *Enterobacterales* infections treated at Renji Hospital, Shanghai Jiao Tong University School of Medicine, between 2022 and 2024. The cohort comprised 1,028 patients categorized into two groups: 262 patients who developed persistent infections and 766 patients whose infections successfully resolved (Fig. 1a). Persistent infection was defined as ongoing clinical and/or microbiological failure for at least 21 days following the initiation of appropriate therapy, documented by at least two positive bacterial cultures.

Patients were included if they were adults (≥18 years old) presenting with a documented, monomicrobial extraintestinal infection caused by an in vitro

carbapenem-susceptible *Enterobacterales* isolate (e.g., *Escherichia coli*, *Klebsiella pneumoniae*, or *Enterobacter cloacae*). Additional inclusion criteria required that patients underwent active screening for carbapenem-resistant *Enterobacterales* (CRE) carriage via rectal swabs upon admission. Furthermore, patients must have received appropriate, targeted antimicrobial therapy adhering strictly to standard hospital dosing protocols, including necessary renal dose adjustments, for a minimum of 48 to 72 hours.

Patients were excluded if their primary infection was caused by a carbapenem-resistant isolate or if they presented with isolated persistent urinary tract infections[43]. To eliminate confounding variables, we further excluded cases featuring polymicrobial infections and those lacking adequate source control, such as undrained abscesses, retained infected hardware, or un-debrided necrotic tissue. Finally, we excluded patients with profound immunosuppression (absolute neutrophil count <500 cells/μL) or those undergoing active induction chemotherapy[44], individuals transitioned to palliative care, and those who experienced early mortality or were discharged within the first 48 to 72 hours before clinical resolution could be accurately evaluated. Following patient stratification, we performed a multivariate risk factor analysis incorporating host characteristics, infection features, microbiological parameters, and baseline fecal CRE surveillance data.

Active surveillance for intestinal CRE carriage

Rectal swabs collected upon admission were directly inoculated onto MacConkey agar containing a 10-μg meropenem disk and incubated aerobically at 37°C for 18

hours. Suspected carbapenem-resistant colonies growing within or near the inhibition zone were sub-cultured for purity. Species identification was performed using matrix-assisted laser desorption/ionization time-of-flight mass spectrometry (MALDI-TOF MS; AutoBio). Isolates identified as *Enterobacterales* underwent antimicrobial susceptibility testing via broth microdilution. Imipenem and meropenem minimum inhibitory concentrations (MICs) were determined and interpreted according to Clinical and Laboratory Standards Institute (CLSI) M07 and M100 (35th edition, 2025) guidelines. Isolates exhibiting resistance to at least one tested carbapenem were classified as carbapenem-resistant *Enterobacterales* (CRE) and retained for subsequent characterization.

Whole genome sequencing and bioinformatic analysis

Clinical *E. coli* and *K. pneumoniae* isolates were sequenced on an Illumina NovaSeq 6000 platform (150-bp paired-end reads). Raw reads were quality-trimmed with Trimmomatic v0.36 and assembled de novo using SPAdes v4.1.0. Antimicrobial resistance genes, plasmid replicons, and multi-locus sequence types (MLST) were identified via the Center for Genomic Epidemiology using ResFinder, PlasmidFinder, and standard MLST schemes[45]. Roary v3.11.2 was used for pan-genome analysis, with core genes defined as those present in ≥95% of isolates. Core-genome single-nucleotide polymorphisms (cgSNPs) were extracted from the alignment using SNP-sites and filtered with VCFtools v0.1.17. A maximum-likelihood phylogenetic tree was constructed from the filtered cgSNP alignment using RAxML-NG v1.1.0

(GTR+G substitution model, 1,000 bootstrap replicates) and visualized in Interactive Tree of Life (iTOL) v6.

Expression and purification of recombinant NDM-5

To maximize soluble expression without altering carbapenemase activity, the *bla*$_{\text{NDM-5}}$ coding sequence lacking the N-terminal signal peptide was cloned into the pCold II vector using the NEBuilder HiFi DNA Assembly Kit (New England Biolabs)[46]. Following Sanger sequencing confirmation, the construct was transformed into *E. coli* BL21(DE3). Cultures were grown in Luria-Bertani broth with 50 μg/mL ampicillin to an OD600 of ~0.5, induced with 0.2 mM IPTG (Yeasen Biotechnology), and incubated at 16°C for 16 h. Cells were harvested by centrifugation and lysed by sonication. Recombinant NDM-5 was purified from the clarified supernatant using nickel-affinity chromatography (QIAGEN), with final protein concentration and purity verified with a BCA Protein Assay Kit (Beyotime) and sodium dodecyl sulphate- polyacrylamide gel electrophoresis (SDS-PAGE), respectively.

Isolation and purification of OMVs

Outer membrane vesicles (OMVs) were isolated from overnight cultures of *E. coli* or *K. pneumoniae* diluted 1:1,000 in 200 mL of Luria-Bertani broth and incubated for 16 h at 37°C (180 rpm). Cells were removed by centrifugation (4,000 × g, 10 min). The supernatants were filtered (0.22-μm) and concentrated using a 100-kDa hollow-fiber ultrafiltration membrane (Millipore). Concentrated supernatants were ultracentrifuged at 174,900 × g for 4 h at 4°C (SW 32 Ti rotor, Beckman Coulter). The resulting

OMVs pellets were resuspended in 4.4 mL of 50% OptiPrep (Axis-Shield), loaded beneath a discontinuous gradient of 40% (4 mL) and 10% (1.6 mL) OptiPrep, and ultracentrifuged at 200,000 × g for 16 h at 4°C (SW 41 Ti rotor). The purified OMVs fraction was collected from the 10%/40% interface[47].

Nanoparticle tracking analysis

OMVs size distribution and concentration were quantified using a NanoSight NS300 instrument (Malvern) equipped with a 488-nm laser and an sCMOS camera. Samples were diluted in sterile PBS to a final concentration of approximately 1×10^8 particles/mL and analyzed according to the manufacturer's protocol.

Transmission electron microscopy

For morphological analysis, 10 µL of the OMVs suspension was adsorbed onto a copper grid for 7 min. Grids were negatively stained with 3% uranyl acetate for 10 s, washed twice with PBS, and air-dried. Images were acquired on an HT7700 transmission electron microscope (Hitachi) operating at 100 kV.

Colloidal gold immunochromatographic assay

The presence of NDM in CREC isolates, purified recombinant NDM-5, and OMVs was evaluated using the NG-Test CARBA 5 assay (NG Biotech). Bacterial colonies were processed according to the manufacturer's instructions. For cell-free samples, 10 µg of purified NDM-5 or 20 µg of total OMVs protein was mixed with the provided extraction buffer. A 50-µL aliquot of each mixture was loaded onto the test cassette

and incubated for 15 min at room temperature before visually confirming the appearance of the NDM-specific and internal control lines.

Western blot analysis

OMVs and bacterial culture fractions were lysed in cold RIPA buffer (Millipore) supplemented with PMSF (Sigma) for 20 min on ice. Protein concentrations were determined using a BCA Protein Assay Kit (Beyotime). Equal amounts of protein (20μg per lane) were denatured in 1×loading buffer at 95°C for 10 min, separated by 12.5% SDS-PAGE, and transferred to 0.2-μm PVDF membranes (Millipore). Membranes were blocked with 5% skim milk in Tris-buffered saline containing 0.05% Tween-20 (TBST) for 1 h at room temperature, followed by overnight incubation at 4 ° C with mouse monoclonal anti-NDM (Biocare Medical, M9161; 1:1,000) or anti-KPC (Biocare Medical, M9171; 1:1,000) primary antibodies. After three washes in TBST, membranes were incubated with an HRP-conjugated goat anti-mouse secondary antibody (Abcam, ab6728; 1:1,000) for 1 h at room temperature. Immunoreactive signals were visualized using enhanced chemiluminescence on an Amersham Imager 600.

Quantification of carbapenemase activity

Carbapenemase activity was quantified by continuously monitoring meropenem hydrolysis at 300 nm[13,48]. Assays were performed at 37°C in 200-μL reactions containing 50 mM HEPES (pH 7.0), 10 μM $ZnSO_4$, and 100 μM meropenem. Reactions were initiated by adding 1-2 μg of total protein from bacterial fractions or

OMVs, and absorbance was recorded for 15 min using a Biotek synergy H1 microplate reader (Agilent). Initial hydrolysis rates (ΔA_{300}/min) were calculated from the linear portion of the curve via linear regression, utilizing meropenem-free samples for background correction. Absolute hydrolysis was determined using the differential molar extinction coefficient of meropenem ($\Delta\varepsilon_{300} = -6{,}500\ M^{-1}\ cm^{-1}$), adjusted for the microplate optical path length. When evaluating antibiotic stress, carbapenemase activity was normalized to the total OMVs particle count determined by NTA. All assays were performed in triplicate.

Meropenem susceptibility testing

Meropenem minimum inhibitory concentrations (MICs) were determined by broth microdilution in cation-adjusted Mueller-Hinton broth using a standard inoculum of ~5×10^5 CFU/mL. Pathogens used for *in vitro* assays were selected from the clinical cohort. Whole-genome sequencing confirmed these isolates lacked carbapenemase genes. To evaluate extracellular protection, purified NDM-5 (10 μg/mL) or OMVs (20 μg/mL total protein) were added prior to bacterial inoculation. Assays included standard antibiotic-free and additive-free controls. Following a 20-h incubation at 37° C, MICs measured in the presence of purified NDM-5 or OMVs were recorded as the lowest drug concentration preventing visible growth and compared against baseline MICs obtained with meropenem alone.

Time-kill assay

Time-kill assays utilized *E. coli* and *K. pneumoniae* clinical isolates with available genomic data, randomly selected from the persistent infection cohort. Mid-log phase cultures were diluted to ~1 × 10^6 CFU/mL. To evaluate extracellular protection, purified NDM-5 (10 μg/mL) or carbapenemase-loaded OMVs (20 μg/mL total protein) were added prior to meropenem (4 μg/mL). Controls included untreated bacteria and bacteria exposed to meropenem alone. Cultures were incubated at 37°C (180 rpm). Aliquots collected at 0, 2, 4, 6, and 8 h were serially diluted in PBS and plated on LB agar. Viable counts (CFU/mL) were determined after 18 h of incubation at 37°C (limit of detection, 10 CFU/mL). All assays were performed in biological triplicate.

Mouse model of intra-abdominal infection and pharmacokinetic analysis

Female C57BL/6J mice (6-8 weeks old) were infected intraperitoneally with 2 × 10^7 CFU of a carbapenem-susceptible *K. pneumoniae* clinical isolate with available genomic data, randomly selected from the persistent infection cohort. Whole-genome sequencing confirmed the isolate lacked carbapenemase genes. Two hours post-infection, mice were randomly assigned to four treatment groups: PBS control, meropenem plus PBS, meropenem plus purified NDM-5, and meropenem plus NDM-loaded OMVs. Meropenem (25 mg/kg) or PBS was administered intravenously, followed 15 min later by PBS, purified NDM-5 (10 μg), or NDM-loaded OMVs (30 μg total protein) according to group assignment. This treatment regimen was repeated at 24 h.

Survival was monitored every 6 h. At 48 h post-infection, surviving mice were euthanized, and blood was collected via retro-orbital bleeding for plasma isolation.

Liver and spleen samples were weighed, homogenized in sterile PBS, and plated on Mueller-Hinton agar to quantify bacterial burden (CFU/g tissue). Additional organ sections were fixed in 4% paraformaldehyde, paraffin-embedded, and stained with hematoxylin and eosin (H&E) for histopathological evaluation.

Separate mouse cohorts were utilized to assess the effects of purified NDM-5 and NDM-loaded OMVs on meropenem pharmacokinetics (PK). Following the 24-h treatment dose, mice (n = 3 per time point per group) were euthanized at 0.5, 1, 2, 4, and 8 h. Plasma meropenem concentrations were quantified using liquid chromatography-tandem mass spectrometry (LC-MS/MS; AB SCIEX Triple Quad 4500MD). PK parameters were determined via non-compartmental analysis, and PK profiles were calculated using an 8-h dosing interval to model standard clinical regimens[35].

Immunogold electron microscopy

OMVs from NDM-producing *E. coli* were fixed 1:1 (v/v) in 4% paraformaldehyde and adsorbed onto carbon-coated grids for 20 min. Grids were washed with PBS, quenched with 50 mM glycine, and blocked overnight at 4 °C in 5% bovine serum albumin (BSA). For immunolabeling, grids were incubated for 1 h at room temperature with mouse anti-LPS (LifeSpan BioSciences, LS-C295816; 1:20) or mouse anti-NDM (Biocare Medical, M9161; 1:20) primary antibodies. Following PBS washes, grids were incubated for 1 h with a colloidal gold-conjugated secondary antibody (Abcam, ab39619; 1:200). Samples were washed sequentially in 0.5% BSA and PBS, post-fixed with 1% glutaraldehyde for 2 min, rinsed with double-distilled

799 water, and counterstained with 2% uranyl acetate for 90 s. Air-dried grids were then
800 examined by transmission electron microscopy.

801 **Isolation of extracellular vesicles from plasma**

802 Extracellular vesicles (EVs) were isolated from human and mouse plasma using
803 differential ultracentrifugation[47,49]. Blood samples were collected into EDTA-coated
804 tubes (BD Biosciences). Plasma was separated at 1,000 × g for 10 min at room
805 temperature, followed by two sequential clearing spins at 2,500 × g for 15 min to
806 remove residual cells and platelets. The supernatant was centrifuged at 10,000 × g
807 for 20 min at 4 °C and passed through a 0.45-μm filter (Sigma) to deplete larger
808 particles. The filtrate was then ultracentrifuged at 120,000 × g for 2 h at 4°C (SW 55
809 Ti rotor, Beckman Coulter). The resulting EV pellet was washed in PBS,
810 ultracentrifuged again at 120,000 × g for 2 h at 4°C, resuspended in 50 μL of PBS,
811 and stored at -80°C until analysis.

812 **Nano-flow cytometry**

813 Extracellular vesicles (EVs) were analyzed using a NanoFCM N30E instrument
814 (NanoFCM). EV samples were diluted to 5 × 10^8 particles/mL in PBS. Aliquots
815 containing 5 × 10^7 particles were incubated with mouse monoclonal anti-LPS
816 (LifeSpan BioSciences, LS-C295816) or anti-NDM (Biocare Medical, M9161)
817 primary antibodies for 60 min at 37°C. Unbound antibodies were removed via two
818 ultracentrifugation washes (120,000 × g, 60 min, 4°C; SW 55 Ti rotor, Beckman
819 Coulter). Pellets were resuspended in PBS and incubated with a Fluor 488-conjugated

goat anti-mouse IgG secondary antibody (Yeasen, 33206ES60) for 60 min at 37°C, followed by two identical ultracentrifugation washes. Final EV pellets were resuspended in 20 μL of PBS. Negative controls included EVs incubated with secondary antibody alone, primary antibody alone, and an isotype-matched mouse IgG (LifeSpan BioSciences, LS-C292295) with the secondary antibody. For data acquisition, 10,000 events were recorded per sample (sheath flow rate, 40 pL/min; sample flow rate, 2 nL/min). The instrument was calibrated using 100-nm fluorescent polystyrene beads. The abundance of LPS- or NDM-positive EVs was calculated as the percentage of fluorescence-positive events relative to the total number of recorded particles.

OMVs-mediated transformation assay

To assess OMVs-mediated horizontal gene transfer, *E. coli* MG1655 *hph* Δ*hsdR* was utilized as the recipient strain[50]. Log-phase recipient cells were harvested by centrifugation and resuspended in PBS supplemented with 0.4% glucose. The cell suspension was mixed with 30 μg (total protein) of purified OMVs from a NDM-producing *E. coli* strain in a 200-μL volume and incubated statically at 37°C for 8 h. Following the addition of 3 mL of LB broth, the culture was incubated overnight at 37°C with shaking (180 rpm). Cells were then pelleted, resuspended in 200 μL of LB broth, and plated on LB agar containing 2 μg/mL meropenem to select for transformants.

Paracellular translocation of OMVs across Caco-2 monolayers

841 Caco-2 cells were cultured in high-glucose DMEM supplemented with 10% FBS, 1%
842 GlutaMAX, 1% non-essential amino acids, and 1% penicillin-streptomycin at 37°C
843 with 5% CO_2. For translocation assays, cells were seeded onto 12-well polycarbonate
844 Transwell inserts (0.4-μm pore size; Corning) at 7.5×10^4 cells/cm² and differentiated
845 for 21 days. To model epithelial injury, monolayers were apically treated with 0%,
846 0.1%, 1%, 3%, or 5% (w/v) dextran sulfate sodium (DSS) (Yeasen Biotechnology) for
847 24 h[15]. Following PBS washes, fresh medium was applied to both compartments, and
848 30 μg of purified *E. coli* OMVs (total protein; ~5×10^{10} particles) was added apically.
849 Parallel inserts without OMVs served as background controls. After a 24-h incubation,
850 the basolateral medium was collected. Translocated particles were quantified by
851 nanoparticle tracking analysis (NTA), utilizing the no-OMVs controls to subtract
852 background particles. To evaluate the translocation of functional NDM, the
853 basolateral medium was ultracentrifuged at 200,000 × g for 2 h at 4°C. The resulting
854 vesicle pellet was resuspended in assay buffer (50 mM HEPES [pH 7.0], 10 μM
855 $ZnSO_4$), and carbapenemase activity was determined by monitoring meropenem
856 hydrolysis at 300 nm, as described above.

857 **Construction of genetically modified strains**

858 Markerless mutants were generated using the pCONJ6H vector, a pCONJ derivative
859 carrying a hygromycin resistance cassette (*hph*)[51]. Approximately 500-bp upstream
860 and downstream flanking regions of each target gene were PCR-amplified and cloned
861 into pCONJ6H using the NEBuilder HiFi DNA Assembly Kit (New England Biolabs).
862 Following conjugal transfer, single transconjugant colonies were selected in LB broth

863 containing 200 μg/mL hygromycin. To counter-select for plasmid excision, cultures
864 were washed, outgrown in plain LB for 4 h at 37°C, and plated on salt-free LB agar
865 supplemented with 10% (w/v) sucrose. Successful allelic replacement was identified
866 by PCR and confirmed by Sanger sequencing.

867 ***In vivo* tracking of mCherry-labeled OMVs using optical imaging**

868 An *E. coli* reporter strain expressing an OmpF-mCherry fusion was constructed by
869 inserting the mCherry coding sequence in-frame at the 3′ end of *ompF* via
870 homologous recombination. Following PCR and sequencing confirmation, mCherry
871 expression and OMVs fluorescence were verified prior to animal experiments. Female
872 C57BL/6J mice (6-8 weeks old) were randomly assigned to four groups (n = 6 per
873 group): control + PBS, control + OMVs, DSS + PBS, and DSS + OMVs. Colitis was
874 induced in the DSS groups by providing 3% (w/v) DSS in the drinking water for 7
875 days, followed by 7 days of regular water. During the second week, mice received
876 either ~1×10^{10} mCherry-labeled OMVs or PBS via daily oral gavage (100 μL) for 7
877 days. On day 14, mice were euthanized, and the small intestine, ovaries, lungs, liver,
878 and kidneys were excised and rinsed in PBS. Fluorescence imaging was performed
879 using an IMAGING 200pro optical system (Indec Bio; excitation 560 nm, emission
880 620 nm). Regions of interest were defined using Raycision Imaging Suite software.
881 Fluorescence intensity was quantified as radiant efficiency
882 [photons/s/cm²/sr/(μW/cm²)] and normalized to PBS-treated controls.

883 **Mouse model of intestinal CREC colonization and DSS-induced colitis**

Female C57BL/6J mice (6-8 weeks old) were orally gavaged daily for 14 days with ~2 × 10^8 CFU of either wild-type CREC or the isogenic Δbla_{NDM} mutant. An NDM-5-producing fecal CREC isolate was randomly selected. To induce colitis, 3% (w/v) DSS was administered in the drinking water from days 8 to 14. Mice (n = 8 per group) were assigned to five groups: untreated control, DSS only, CREC only, CREC with DSS, and Δbla_{NDM} CREC with DSS. Intestinal colonization was confirmed by plating fecal homogenates collected on days 7 and 14 onto selective agar, with counts expressed as $\log_{10}$ CFU/g. On day 14, plasma was isolated from retro-orbital blood samples (3,000 × g, 15 min, 4°C) to quantify procalcitonin (PCT) via ELISA (R&D Systems). Plasma LPS and NDM-positive vesicles were determined with Nano-flow cytometry, as described above. Colons were excised and measured. Distal colon segments were fixed in 4% paraformaldehyde, paraffin-embedded, and H&E-stained for histopathological evaluation.

Separate cohorts were utilized for pharmacokinetic assessments. On day 14, mice received a single intravenous dose of meropenem (100 mg/kg). Plasma was collected at 0.5, 1, 2, 4, and 8 h post-administration (n = 3 per time point per group), and meropenem concentrations were quantified by LC-MS/MS. Pharmacokinetic parameters were calculated via non-compartmental analysis.

Quantitative proteomic analysis of outer membrane vesicles

OMVs were isolated from CREC cultured in LB broth with or without 4 μg/mL meropenem (n=3 biological replicates). OMV pellets were lysed in SDT buffer (4% SDS, 100 mM Tris-HCl [pH 8.0], 100 mM DTT), boiled for 3 min, sonicated for 2

min, and cleared by centrifugation (16,000 × g, 20 min, 4°C). Protein concentrations were determined by BCA assay, with sample integrity verified by SDS-PAGE. Proteins were processed via filter-aided sample preparation (FASP). Following reduction, samples were loaded onto 10-kDa centrifugal filters, washed with UA buffer (8 M urea, 150 mM Tris-HCl [pH 8.0]), alkylated with 50 mM iodoacetamide, and digested with trypsin (Promega; 1:25 w/w) for 16 h at 37°C. Peptides were C18-desalted, vacuum-dried, reconstituted in 0.1% formic acid, and analyzed on a Vanquish Neo UHPLC system coupled to an Orbitrap Astral mass spectrometer (Thermo Scientific). Separation utilized a µPAC Neo High Throughput column with a 15-min acetonitrile gradient (2 µL/min). Data-independent acquisition (DIA) spanned an m/z range of 380-980. Raw data were processed with DIA-NN v1.8 against the UniProt *E. coli* database (Taxonomy ID 562). Differential abundance was defined as a fold change of ≥1.5 or ≤0.67 with $P < 0.05$.

RNA extraction and quantitative reverse-transcription PCR

Total RNA was extracted from bacterial cultures using the MolPure Bacterial RNA Kit (Yeasen Biotechnology) and reverse-transcribed (500 ng per sample) into cDNA using the PrimeScript RT Reagent Kit (TaKaRa). Quantitative PCR was performed on a 7500 Real-Time PCR System (Applied Biosystems) with Hieff UNICON Universal Blue qPCR SYBR Green Master Mix (Yeasen Biotechnology). Relative gene expression was normalized to *rpoB* and calculated via the $2^{-\Delta\Delta Ct}$ method. All samples were analyzed in technical triplicate.

Plasmid copy number determination

The copy number of the *bla*$_{NDM}$-carrying plasmid was determined by qPCR, calculated as the ratio of plasmid-borne *bla*$_{NDM}$ to the single-copy chromosomal reference gene *rpoB*[52]. Absolute copy numbers for each sample were interpolated from standard curves generated using 10-fold serial dilutions of purified pGM-T vectors (Tiangen Biotech) carrying either the *bla*$_{NDM}$ or *rpoB* amplicons. All reactions were performed in technical triplicate.

Mouse model of CREC colonization, colitis, and secondary pneumonia

Female C57BL/6J mice (6-8 weeks old) were orally gavaged daily for 14 days with ~1 × 10^8 CFU of CREC to establish intestinal colonization. Colitis was induced by supplementing the drinking water with 3% (w/v) DSS from days 8 to 14. On days 15 and 16, isoflurane-anesthetized mice were intranasally inoculated with ~5 × 10^7 CFU of a carbapenem-susceptible *K. pneumoniae* strain, which was selected from the clinical cohort as described above. Prior to treatment on day 17, mice were randomly assigned to four groups (n = 8 per group) and administered intravenous PBS, meropenem (25 mg/kg), amikacin (15 mg/kg), or aztreonam-avibactam (50/12.5 mg/kg) once daily on days 17 and 18. Six hours after the final dose, mice were euthanized. Whole blood and homogenized lung tissues were plated on Mueller-Hinton agar to quantify bacterial burdens. Plasma isolated from retro-orbital blood was analyzed for LPS- and NDM-positive vesicles via nano-flow cytometry, and procalcitonin (PCT) levels were determined by ELISA.

Separate cohorts were used for pharmacokinetic studies (n = 3 per time point per group). Following the final antibiotic dose on day 18, mice were euthanized at 0.5, 1,

2, 4, and 8 h. Serum antibiotic concentrations were quantified by LC-MS/MS, and pharmacokinetic parameters were derived via non-compartmental analysis.

Statistics

Statistical analyses were performed using GraphPad Prism 10 (GraphPad Software). All independent experiments included at least three biological replicates. Univariate and multivariate logistic regression models were used to identify independent clinical predictors of persistent infection. Data were presented as mean ± SD unless otherwise indicated. Normality was assessed using the Shapiro-Wilk test. Two-group comparisons were evaluated using unpaired two-sided Student's t-tests. Comparisons among three or more groups were analyzed utilizing one-way ANOVA with Tukey's post hoc test, or the Kruskal-Wallis test with Dunn's post hoc test, as appropriate based on normality. Associations between continuous variables were evaluated using Pearson correlation analysis. The effect size, reported as Pearson's correlation coefficient (r), was calculated from the coefficient of determination (r^2) derived via simple linear regression. Categorical variables were compared using Fisher's exact test or the $\chi 2$ test. Following acclimation, animals were randomly assigned to experimental groups using computer-generated random numbers in Microsoft Excel.

References

1. Chea, N. *et al.* Health care-associated infections in U.S. hospitals, 2023 versus 2015. *N. Engl. J. Med.* **395**, 255-266 (2026).

2. Xi, J. *et al.* A nationwide genomic surveillance study of Gram-negative

bacteria causing community- and hospital-acquired bloodstream infections in China. *J. Infect.* **92**, (2026).

3. Balaban, N. Q. *et al.* Definitions and guidelines for research on antibiotic persistence. *Nat. Rev. Microbiol.* **17**, 441-448 (2019).

4. Ciofu, O., Moser, C., Jensen, P. Ø. & Høiby, N. Tolerance and resistance of microbial biofilms. *Nat. Rev. Microbiol.* **20**, (2022).

5. Müller, M., Dela Peña, A. & Derendorf, H. Issues in Pharmacokinetics and pharmacodynamics of anti-infective agents: distribution in tissue. *Antimicrob. Agents Chemother.* **48**, 1441-1453 (2004).

6. Campos-Madueno, E. I. *et al.* Intestinal colonization with multidrug-resistant *Enterobacterales*: screening, epidemiology, clinical impact, and strategies to decolonize carriers. *Eur. J. Clin. Microbiol. Infect. Dis.* **42**, 229-254 (2023).

7. Henoun Loukili, N. *et al.* Time to intestinal clearance of carbapenemase-producing *Enterobacterales* in hospital patients: a longitudinal retrospective observational cohort study. *J. Hosp. Infect.* **135**, 4-10 (2023).

8. Lyu, Y. Y. *et al.* Phenotypic and genotypic characterization of colonization and infection with carbapenem-resistant *Enterobacteriaceae*: A prospective cohort study in China. *J. Infect.* **92**, (2026).

9. Gorrie, C. L. *et al.* Gastrointestinal Carriage Is a Major reservoir of *Klebsiella pneumoniae* infection in intensive care patients. *Clin. Infect. Dis.* **65**, 208-215 (2017).

10. Toyofuku, M., Schild, S., Kaparakis-Liaskos, M. & Eberl, L. Composition and functions of bacterial membrane vesicles. *Nat. Rev. Microbiol.* **21**, 415-430 (2023).

11. Zhang, X. *et al.* Carbapenemase-loaded outer membrane vesicles protect *Pseudomonas aeruginosa* by degrading imipenem and promoting mutation of antimicrobial resistance gene. *Drug Resist. Updat.* **68**, 100952 (2023).

12. González, L. J. *et al.* Membrane anchoring stabilizes and favors secretion of New Delhi metallo-β-lactamase. *Nat. Chem. Biol.* **12**, 516-522 (2016).

13. Martínez, M. M. B., Bonomo, R. A., Vila, A. J., Maffía, P. C. & González, L. J. On the offensive: the role of outer membrane vesicles in the successful dissemination of New Delhi Metallo-β-lactamase (NDM-1). *MBio* **12**, e0183621 (2021).

14. Li, L. *et al.* NDM-5-carried outer membrane vesicles impair the efficacy of antibiotics against bacterial infections. *Antimicrob. Agents Chemother.* **69**, e0180524 (2025).

15. Tulkens, J. *et al.* Increased levels of systemic LPS-positive bacterial extracellular vesicles in patients with intestinal barrier dysfunction. *Gut* **69**, 191-193 (2020).

16. Ou, Z. *et al.* Single-particle analysis of circulating bacterial extracellular vesicles reveals their biogenesis, changes in blood and links to intestinal barrier. *J. Extracell. vesicles* **12**, e12395 (2023).

17. Kumarasamy, K. K. *et al.* Emergence of a new antibiotic resistance mechanism in India, Pakistan, and the UK: A molecular, biological, and epidemiological study. *Lancet Infect. Dis.* **10**, 597-602 (2010).

18. Timsit, J.-F. *et al.* Antibiotic therapy for severe bacterial infections. *Intensive Care Med.* **51**, 1867-1885 (2025).

19. Tripathi, A. *et al.* Identification of human zonulin, a physiological modulator of tight junctions, as prehaptoglobin-2. *Proc. Natl. Acad. Sci. U. S. A.* **106**, 16799-16804 (2009).

20. Dahlgren, D. & Lennernäs, H. Review on the effect of chemotherapy on the intestinal barrier: Epithelial permeability, mucus and bacterial translocation. *Biomed. Pharmacother.* **162**, 114644 (2023).

21. Devarakonda, S. *et al.* Low-grade intestinal inflammation two decades after pelvic radiotherapy. *eBioMedicine* **94**, 104691 (2023).

22. Sawaed, J. *et al.* Antibiotics damage the colonic mucus barrier in a microbiota-independent manner. *Sci. Adv.* **10**, 1-12 (2024).

23. Tatge, L., Solano Fonseca, R. & Douglas, P. M. A framework for intestinal barrier dysfunction in aging. *Nat. Aging* **3**, 1172-1174 (2023).

24. Razew, A. *et al.* Quantifying outer membrane permeability to β-lactam antibiotics using outer membrane vesicles that protect antibiotic-susceptible bacteria. *Nat. Commun.* **17**, 1-12 (2026).

25. Bajaj, H. *et al.* Molecular Basis of filtering carbapenems by porins from

β-lactam-resistant clinical strains of *Escherichia coli*. *J. Biol. Chem.* **291**, 2837-2847 (2016).

26. Kaderabkova, N. *et al.* The biogenesis of β-lactamase enzymes. *Microbiol. (United Kingdom)* **168**, 001217 (2022).

27. David, S. *et al.* Widespread emergence of OmpK36 loop 3 insertions among multidrug-resistant clones of *Klebsiella pneumoniae*. *PLoS Pathog.* **18**, 1-23 (2022).

28. López, C., Delmonti, J., Bonomo, R. A. & Vila, A. J. Deciphering the evolution of metallo-β-lactamases: A journey from the test tube to the bacterial periplasm. *J. Biol. Chem.* **298**, 101665 (2022).

29. Tacconelli, E. *et al.* ESCMID-EUCIC clinical guidelines on decolonization of multidrug-resistant Gram-negative bacteria carriers. *Clin. Microbiol. Infect.* **25**, 807-817 (2019).

30. Zeng, M. *et al.* Guidelines for the diagnosis, treatment, prevention and control of infections caused by carbapenem-resistant gram-negative bacilli. *J. Microbiol. Immunol. Infect.* **56**, 653-671 (2023).

31. Rossolini, G. M., Arhin, F. F. & Kantecki, M. In vitro activity of aztreonam-avibactam and comparators against Metallo-β-Lactamase-producing *Enterobacterales* from ATLAS Global Surveillance Program, 2016-2020. *J. Glob. Antimicrob. Resist.* **36**, 123-131 (2024).

32. Li, P. *et al.* Circulating outer membrane vesicles from gut-colonized

carbapenem-resistant Enterobacterales degrade antibiotics and promote bacterial survival. *Infect. Drug Resist.* **18**, 6509-6519 (2025).

33. Hendrix, A. & De Wever, O. Systemically circulating bacterial extracellular vesicles: origin, fate, and function. *Trends Microbiol.* **30**, 213-216 (2022).

34. Gatti, M., Cojutti, P. G. & Pea, F. Impact of attaining aggressive vs. conservative PK/PD target on the clinical efficacy of beta-lactams for the treatment of Gram-negative infections in the critically ill patients: a systematic review and meta-analysis. *Crit. Care* **28**, 123 (2024).

35. Kitzes-Cohen, R., Farin, D., Piva, G. & De Myttenaere-Bursztein, S. A. Pharmacokinetics and pharmacodynamics of meropenem in critically ill patients. *Int. J. Antimicrob. Agents* **19**, 105-10 (2002).

36. Wang, Q. *et al.* Expansion and transmission dynamics of high risk carbapenem-resistant *Klebsiella pneumoniae* subclones in China: An epidemiological, spatial, genomic analysis. *Drug Resist. Updat.* **74**, (2024).

37. Budia-Silva, M. *et al.* International and regional spread of carbapenem-resistant *Klebsiella pneumoniae* in Europe. *Nat. Commun.* **15**, (2024).

38. Feilong, Z., Wenting, Y., Binghuai, L. & Bin, C. Dynamic global variation in resistance and hypervirulence of carbapenem-resistant *Klebsiella pneumoniae* between 2010 and 2023. *J. Infect.* **90**, 106493 (2025).

39. Li, T. *et al.* Adaptive evolution of extensive drug resistance and persistence in epidemic ST11 KPC-producing *Klebsiella pneumoniae* during antimicrobial

chemotherapy. *Antimicrob. Agents Chemother.* **69**, e0123524 (2025).

40. Argimón, S. *et al.* Rapid genomic characterization and global surveillance of *Klebsiella* using Pathogenwatch. *Clin. Infect. Dis.* **73**, S325-S335 (2021).

41. Wong, J. L. C. *et al.* OmpK36-mediated carbapenem resistance attenuates ST258 *Klebsiella pneumoniae* in vivo. *Nat. Commun.* **10**, (2019).

42. Torabian, P. *et al.* Effect of clinically relevant antibiotics on bacterial extracellular vesicle release from *Escherichia coli*. *Int. J. Antimicrob. Agents* **65**, (2025).

43. Timm, M. R., Russell, S. K. & Hultgren, S. J. Urinary tract infections: pathogenesis, host susceptibility and emerging therapeutics. *Nat. Rev. Microbiol.* **23**, 72-86 (2025).

44. Ramirez, J. A. *et al.* Treatment of community-acquired pneumonia in immunocompromised adults: A consensus statement regarding initial strategies. *Chest* **158**, 1896-1911 (2020).

45. Florensa, A. F., Kaas, R. S., Clausen, P. T. L. C., Aytan-Aktug, D. & Aarestrup, F. M. ResFinder – an open online resource for identification of antimicrobial resistance genes in next-generation sequencing data and prediction of phenotypes from genotypes. *Microb. Genomics* **8**, 1-10 (2022).

46. Cheng, Z. *et al.* Evolution of New Delhi metallo-β-lactamase (NDM) in the clinic: Effects of NDM mutations on stability, zinc affinity, and mono-zinc activity. *J. Biol. Chem.* **293**, 12606-12618 (2018).

47. Gao, Q. *et al.* Dynamic Profiling of Lipoteichoic Acid (LTA) and/or lipopolysaccharide (LPS) positive extracellular vesicles in plasma as diagnostic and prognostic biomarkers for bacterial infection. *Adv. Sci. (Weinheim, Baden-Wurttemberg, Ger.* **06613**, e06613 (2025).

48. Palacios, A. R. *et al.* The reaction mechanism of metallo-lactamases is tuned by the conformation of an active-site mobile loop. *Antimicrob. Agents Chemother.* **63**, 1-15 (2019).

49. Gao, Q. *et al.* Dynamic profiling of penicillin-binding protein 2a (PBP2a)-positive extracellular vesicles: Implications for early diagnosis and treatment monitoring of methicillin-resistant *Staphylococcus aureus* infections. *J. Extracell. vesicles* **14**, e70111 (2025).

50. Wang, X. *et al.* Nosocomial dissemination of $bla_{\text{IMP-4}}$ among *Klebsiella pneumoniae* by horizontal gene transfer and clonal spread: the epidemic IncN plasmids and the emerging high-risk IMP-4-producing ST101 clone. *J. Antimicrob. Chemother.* **78**, 2890-2894 (2023).

51. Shen, Z. *et al.* Outer membrane vesicles mediating horizontal transfer of the epidemic $bla_{\text{OXA-232}}$ carbapenemase gene among *Enterobacterales*. *Emerg. Microbes Infect.* **13**, 1-11 (2024).

52. Shen, Z. *et al.* High ceftazidime hydrolysis activity and porin OmpK35 deficiency contribute to the decreased susceptibility to ceftazidime/avibactam in KPC-producing *Klebsiella pneumoniae*. *J. Antimicrob. Chemother.* **72**,

1930-1936 (2017).

Data availability

Genomic sequencing data have been deposited in the NCBI's SRA database under Bioproject number PRJNA1554080. Additional data that support the findings of this study are available from the corresponding author, Zhen Shen, upon request (zhenshen@shsmu.edu.cn).

Acknowledgements

This study was supported by National Key Research and Development Program of China (2025YFC3409100), National Natural Science Foundation of China (82572615, 82272374), and Shanghai Pujiang Program (22PJ1409600). The funders had no role in study design, data collection and analysis, decision to publish, or preparation of the manuscript.

Author contributions

G.X., C.W., and Z.S. collected clinical strains and performed whole-genome sequencing. J.H., Z.Y., X.Z., and Z.S. established cell models and performed animal studies. Y.Z., J.Z., J.Q., and H.Z. retrospectively analyzed the clinical cohort. Q. G, T. C. and H. W. performed vesicle analysis. G.X. and Y.S. performed LC-MS/MS tests for meropenem concentrations determination. G.X. and Z.S. constructed genetically modified strains. G.X, H.W., M.L. and Z.S. planned, and M.L. supervised experiments. G.X., M.L. and Z.S. analyzed the data. Z.S. wrote the paper.

Competing interests

The authors declare no competing interests.

Supplementary Files

This is a list of supplementary files associated with this preprint. Click to download.

- Extendeddata.pdf